Single-molecule nano-optics at low temperature

Inauguraldissertation

zur

Erlangung der Würde eines Doktors der Philosophie

vorgelegt der

Philosophisch-Naturwissenschaftlichen Fakultät

der Universität Basel

von

JACQUELINE YVONNE PAULA BUTTER

aus Heemstede (Niederlande)

BASEL, 2006

Genehmigt von der Philosophisch-Naturwissenschaftlichen Fakultät
auf Antrag von:

Prof. Dr. H.-J. Güntherodt,
Prof. Dr. B. Hecht,
Prof. Dr. D. Klostermeier,

Basel, den 4. April 2006

Prof. Dr. H.-J. Wirz, Dekan

Contents

Acknowledgements

I want to thank all the people with whom I spent the last 4 years, when I was working on the experiments that are described in this thesis.

First of all, I want to thank Prof. B. Hecht for giving me the opportunity to do my PhD in his group and for helpful discussions and experimental support during all these years.

I'm very grateful to Prof. D. Klostermeier for kindly accepting the role of co-referee on my thesis.

Many thanks to Prof. C. Weder (Case Western Reserve University, Cleveland, Ohio) for stimulating discussions and comments during the work on the characterisation of the stretched films of terrylene in linear low-density polyethylene, and to his PhD student, B. R. Crenshaw, for preparing the samples. These samples were vital for the absorption experiment.

I would also like to thank Senta M. Karotke, with whom I shared the experimental set up. It was particularly useful to work together especially in the beginning, when we had to re-build the set up. Many thanks for all those moments that you helped me whenever more than two hands were needed in the lab.

I would like to thank in particular Tatiana Latychevskaia, Prof. D. W. Pohl, Andreas Lieb and Julien Toquant for stimulating discussions on various parts of the work described in this thesis; Wouter J. van Drunen (Universität Hannover) for sending me (electronic) copies of all those articles that I needed for writing my thesis to which I didn't have access in Basel and for explaining me which fundamental parts of my work were not obvious for people working on a related but distinctly different subject; Christine E. Nattrass (Yale University) for checking and correcting the

English language in the final version of my thesis. Many thanks to Thomas Braun for help with Igor Pro.

I would also like to acknowledge all other current and previous members of the nano-optics group: Peter Mühlschlegel, Rabah Mouras, Javad N. Farahani, H.-J. Eisler and Yoriko Lill.

I want to thank the people of the Mechanische Wekstatt for making the mechanical parts of the improved SNOM head and occasionally some other parts of the set up, the Electronische Werkstatt for repair of electronic devices, especially the high voltage amplifiers, and in particular W. Roth for providing me with helium and accepting changes in the amounts needed, even on very short notice.

And finally, I want to thank my family and friends for their continuous support during the last 4 years.

Summary

The work presented in this thesis involves experiments on single molecules at low temperature. At low temperature, many disturbing temperature activated processes are frozen out, resulting in extremely sharp zero-phonon lines in the fluorescence excitation spectra of certain molecule-matrix systems. The presence of sharp absorption lines is accompanied by the fact that the absorption cross-section is significantly increased, approaching a value of about 10% of the theoretical limit for an oscillating dipole.

The first part of this thesis provides background information for understanding the experimental results. It introduces the energy level scheme of a single molecule in a solid matrix at low temperature, the methods to get down to the single-molecule level, the requirements for a molecule-matrix system for single-molecule spectroscopy, the absorption cross-section and saturation. After this theoretical part, the experimental techniques used for the experiments in this thesis, confocal microscopy and aperture scanning near-field optical microscopy, are discussed.

This theoretical part is followed by an experimental part, which describes the combined home-built confocal and aperture scanning near-field optical microscope working at 1.8 K in a helium bath cryostat. It starts with a general overview, followed by detailed descriptions of the most important parts of the set up. The last part of the experimental section describes the preparation of the two different samples used in these studies: terrylene doped into crystals of *p*-terphenyl and terrylene in a stretched film of linear low-density polyethylene.

The second part of this thesis describes the experimental results. It starts with a study of the imaging properties of single molecules at low temperature as a function of excitation frequency and excitation intensity. Molecules are imaged at several spectral positions on their resonance curve. The spot sizes of single molecules

appear increased in resonance compared to the out-of-resonance values and increase with excitation intensity. With the help of Monte Carlo simulations, addressing the measured spot size as a function of detuning (i.e. decreasing signal-to-background ratio) and as a function of intensity, the observed effects could be attributed to pronounced saturation effects in single-molecule imaging. In fact, the spot size of a single molecule turns out to increase with intensity, even below saturation.

After this first experiment, the main experiment of this thesis is described. It starts with the characterisation of a new sample for single-molecule spectroscopy at low temperature, terrylene in a stretched film of linear low-density polyethylene. Terrylene molecules in a stretched film of linear low-density polyethylene are all oriented along the stretching direction and show sufficient spectral stability. The degree of orientation turns out to include all three dimensions. The molecules all have their transition dipole moments aligned in the sample plane, which leads to a maximised absorption cross-section. The maximised absorption cross-section of the terrylene molecules makes this sample a good candidate for single-molecule detection by absorption. Single molecule detection by absorption is the main experiment described in this thesis. Despite the conceptual ease of performing a bulk absorption experiment, single-molecule detection by absorption is often considered hardly possible: the excitation and emission wavelength are exactly the same and the detector is directly exposed to high intensity laser light. Single-molecule detection by absorption exploits the fact that the coherent part of light emitted by the molecule can interfere in the far field with the excitation light. Due to a phase difference between the light scattered resonantly by the molecule and the reflected excitation light, a dispersive signal is observed on scanning the excitation frequency over the resonance of a single molecule. Single molecules are thus detected in absorption as dispersive features. Absorption and fluorescence excitation spectra are recorded simultaneously. From fluorescence excitation spectra, the exact spectral position and line width of single molecules were determined, which facilitated the analysis of the absorption spectra. Dynamical features, like blinking and spectral jumping, are observed. From the amplitudes of the absorption signal and the line width of the signals, a negative correlation between line width and amplitude was found. This confirms the physical principle that the amount of coherently scattered light decreases upon saturation or due to dephasing. Unfortunately, the signal-to-background ratio of absorption spectra is still rather low compared to fluorescence excitation spectra. A method to improve the signal-to-background ratio could be to go to near-field excitation.

The last experimental chapter describes aperture scanning near-field optical microscopy and spectroscopy at 1.8 K. Near-field optical imaging of single molecules in fluorescence is demonstrated for the first time, as well as a direct comparison between near-field and confocal fluorescence excitation spectra. Differences between these spectra are explained in terms of orientation and position of the transition dipole moment of the single molecules with respect to the aperture tip.

Finally, possible future experiments following the line of experiments described in this thesis are presented in the outlook.

1. Introduction

The detection of single molecules in a solid at cryogenic temperature by absorption in 1989 [1] and by fluorescence in 1990 [2] opened the wide field of single-molecule spectroscopy. The detection of only a single molecule at a time allowed for the first time measurements of not only the mean but also the distribution of the observable of interest (e.g. orientation or line-width), which was obscured in ensemble spectroscopy. Typically, the concentration of single fluorescent guest molecules is extremely low compared to the concentration of host molecules, such that they can be considered impurities in the host matrix. The high sensitivity of the molecular zero-phonon line towards changes in the local environment of the fluorescent guest molecules can be exploited to probe the structure and low temperature dynamics of the matrix materials (for reviews see [3–8]). To probe the structure of matrix materials, the orientation of single molecules is measured as a function of spectral and spatial position. Common matrices for such studies are, e.g., Shpol'skii systems or polymers. Dynamics of matrix materials are often observed in spectral instabilities of the guest molecule in the host environment, leading to discontinuous jumps in the resonance frequency of a guest molecule. Such studies could demonstrate for the first time the existence of tunneling two-level systems.

In highly ordered materials, like single crystals, the distribution of spectroscopic parameters due to environmental influences can be minimised. As a consequence, single molecules at cryogenic temperatures behave like nearly ideal two-level quantum systems that are rigidly fixed in space. The latter feature makes them attractive model systems for quantum optical experiments (for reviews see [3, 4, 9]).

The first observation of single molecules at room temperature followed later, using aperture scanning near-field optical microscopy [10] with near-field excitation and far-field detection. The scanning near-field optical microscope was invented in 1984 [11] after the scanning tunnelling microscope in 1982 [12] and followed by the atomic force microscope in 1987 [13, 14]. The best resolution claimed with scanning near-field optical microscopy using aperture probes is on the order of ~ 10 nm [15], which is far beyond the diffraction limit, but not as good as the atomic resolution obtained in scanning tunnelling microscopy and atomic force microscopy [12, 14]. However, fundamental differences between the applicability of these techniques exist, namely, the scanning tunnelling microscope is limited to conducting samples, whereas the atomic force microscope measures the total forces between a sample and a cantilever tip. The aperture scanning near-field optical microscope on the other

hand is used to excite fluorescent molecules or particles close to (or at) the sample surface. The fluorescence or scattered light from these molecules or particles gives information on the chemical composition of the sample.

The aim to achieve highest possible optical resolution triggered further development of the scanning near-field optical microscope, leading to near-field single-molecule spectroscopy at cryogenic temperature in 1994 [16]. Unfortunately, no imaging of single molecules was achieved. Another interesting point would have been a direct comparison of near-field optical spectroscopy to confocal spectroscopy on the same spatial position of the sample to demonstrate directly the increase of resolution due to a decrease in excitation volume.

However, at low temperature, most of the experiments are still performed using far-field optical techniques. Unanswered fundamental questions that could be addressed with single-molecule spectroscopy at low temperature often don't require the use of a scanning near-field optical microscope. Besides, the use of scanning near-field optical microscopy at low temperature seems to be technically problematic. The experiments that are described in this thesis deal with saturation effects in the images of single molecules, single-molecule detection by absorption and scanning near-field optical microscopy and spectroscopy of single molecules at 1.8 K.

Chapter 2 introduces the concepts of single-molecule spectroscopy at low temperature needed to understand the experiments that are described in this thesis. The energy-level scheme, the methods to get down to the single-molecule level, the requirements for the molecule-matrix system, the absorption cross-section of a single molecule and the saturation properties are explained. It also points out the differences between fluorescence excitation and absorption spectroscopy. After this theoretical part, the most important properties of the experimental techniques used in the experiments described in this thesis, confocal microscopy and aperture scanning near-field optical microscopy, are discussed.

The experimental apparatus is presented in chapter 3. It starts out with an overview of the whole set up and is followed by more detailed information on some separate parts of the set up. The last part of this chapter summarises the sample preparation of the two different molecule-matrix systems that were used in the experiments: terrylene in *p*-terphenyl and terrylene in a stretched film of linear low-density polyethylene.

The accuracy with which positions of single molecules can be determined in three dimensions is much better than the diffraction limit, as was shown at low temperatures in Ref. [17–20]. Position determination accuracy in two dimensions is applied in many experiments at room temperature like in biophysics [21, 22]. Contrary to position determination accuracy, little attention has been paid to the spot size of a single molecule. The spot size of a single molecule is studied in chapter 4. The experiments deal with the imaged spot size of a single molecule at low temperature as a function of excitation intensity and excitation frequency, respectively. To check the validity of the results, Monte Carlo simulations were performed. The measured spot size as a function of excitation intensity sheds light on the influences of saturation on optical imaging. A strong increase in the spot size was found. The same holds for the measured spot sizes of single molecules under excitation intensities below the saturation level. It turns out that even at intensities below saturation, the effects of saturation are already visible in a series of images of the same molecule while tuning the excitation frequency through the absorption line of the molecule. This also means that by imaging a molecule in resonance and out of resonance, eventual saturation effects can be observed immediately in the difference in spot size. Even from only one image of a single molecule, it would be possible to determine the saturation intensity and maximum emission rate by fitting with the appropriate function, which takes into account the deviations from a Gaussian spot as a function of intensity.

The main experiment of the work in this thesis, single molecule detection by absorption, is described in chapter 5. It starts with the desired properties of the "ideal" sample for single molecule detection by absorption, followed by the characterisation of the new sample for low-temperature spectroscopy: terrylene in a stretched film of linear low-density polyethylene. After that, simultaneous detection of single molecules by fluorescence and absorption is presented. Absorption spectroscopy makes use of the interference between the light scattered resonantly by the molecule and a weak reflection of laser light from the sample surface. Absorption signals thus show a dispersive behaviour. The simultaneously recorded fluorescence excitation spectra on the other hand provide direct information on the spectral position of the resonance frequency and line width of a single molecule. Dynamical processes like blinking and spectral jumping of single molecules are observed in both detection channels. In particular, molecules are observed that do not emit detectable Stokes-shifted fluorescence but show a strong absorption signal. The "noisy" appearance

of the absorption spectra is caused by the dynamics of single molecules and should not be misinterpreted as system noise. Nevertheless the signal-to-background ratio in absorption spectra is rather poor, compared to the simultaneously recorded fluorescence excitation spectra. A method to improve the signal-to-noise ratio obtained in the absorption experiment could be to go to near-field excitation. However, aperture scanning near-field optical microscopy is not yet a well-established technique at temperatures of $\sim$ 2 K. Chapter 6 explores aperture scanning near-field optical microscopy and spectroscopy on single molecules at cryogenic temperature. Near-field imaging of single molecules in fluorescence at low temperature is demonstrated for the first time as well as a direct comparison between near-field and confocal fluorescence excitation spectra of single molecules. Differences between these spectra are explained in terms of orientation and position with respect to the aperture.

Finally, possible future experiments following the line of the experiments described in this thesis are presented in the outlook.

2. Fundamentals of single-molecule spectroscopy

The first part of this chapter describes the basic properties of single-molecule spectroscopy at low temperature. It explains the energy-level diagram, the methods that are used to detect single molecules, the requirements for the molecule-matrix system and the effect of saturation. It provides a background for the experiments that are described in this thesis.

The second part focuses on the experimental techniques that were used to study single molecules at cryogenic temperature: the confocal microscope and the aperture scanning near-field optical microscope. The basic principles are described with an emphasis on the differences between the techniques.

2.1 Single molecules at cryogenic temperature

2.1.1 Physical principles

The energy-level scheme of a single molecule embedded in a matrix at cryogenic temperature is depicted as a three-level system consisting of the (electronic) singlet ground state S_0, the first (electronic) singlet excited state S_1 and a triplet state T_1. Additionally, vibrational states are on top of all these levels. Various transitions are possible between these states, as is shown in the so-called Jablonski diagram in Fig. 2.1. Radiative transitions are represented by solid arrows, while dashed arrows indicate non-radiative transitions. Excitations can involve electronic, vibrational and phonon states. In most low-temperature experiments, single molecules are excited resonantly from the lowest vibrational level of the singlet ground state S_0 into the lowest vibrational level of the first singlet excited state S_1. This transition is often referred to as the 0-0 transition and is a purely electronic zero-phonon line [23]. In the case of impurity molecules in crystals at ~ 2 K, the line width of this line is close to the life-time limited value, as temperature induced processes are frozen out. Zero-phonon absorption lines are excitations not involving phonons. Absorptions involving phonons are blue-shifted with respect to the zero-phonon line and build up the broad phonon wing of the line. Zero-phonon lines also exist between the singlet ground state and the vibrational levels of the first singlet excited state. After absorption into one of the vibrational levels of the S_1 state, rapid decay (via phonons) will occur to the lowest vibrational level of the S_1 state, from which radiative decay to the ground state can take place (Kasha's rule). Typically the zero-phonon line of vibrational sidelines is three orders of magnitude broader than the zero-phonon line of the 0-0 transition.

After excitation to the S_1-state, the molecule can decay to the ground state by emission of a photon. Emission of a photon of exactly the same wavelength as the excitation is called "resonance fluorescence". Decay to a vibrational level on the electronic ground state occurs by emission of a photon with a longer wavelength (smaller energy) and is called "Stokes-shifted fluorescence". Further de-excitation then takes place via non-radiative processes, in which the excess electronic excitation is directly converted into heat by the creation of phonons. Non-radiative decay from the S_1 state is possible by the creation of a large number of phonons. This process is

called "internal conversion" (not shown). Alternatively, the molecule can undergo a (spin forbidden) transition to the triplet state. Spin-orbit coupling allows for — normally spin forbidden — non-radiative transitions between iso-energetic vibrational levels of electronic states, called "intersystem crossing". Intersystem crossing to the triplet state is followed by non-radiative transitions to the triplet ground state by the creation of phonons. From the triplet ground state, the molecule can either undergo a radiative transition to the singlet ground state (called "phosphorescence") or a non-radiative transition via intersystem crossing to a vibrational level of the singlet ground state. Since transitions between states of different multiplicity are spin forbidden, they take place with low probability.

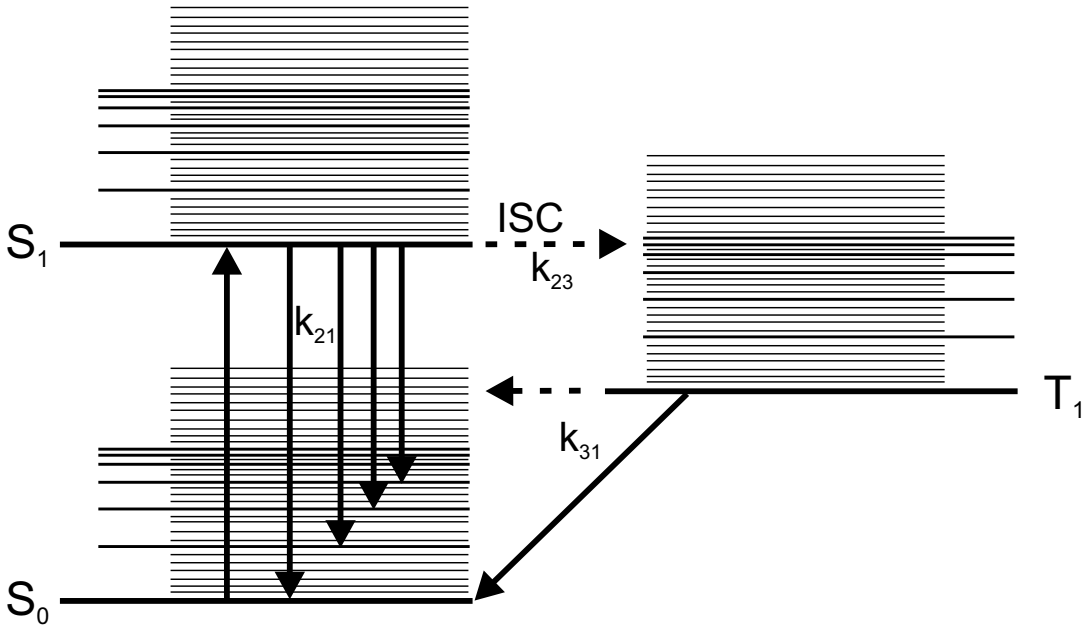

Figure 2.1: *Jablonski diagram. The lowest energy levels of each state are indicated by a thick solid line. Lines marked with ν in the singlet states denote vibrational levels. Thinnest lines are phonon states of the host. Inter-system crossing (ICS) and decay rates (k_{21}, k_{23}, k_{31}) are indicated. Radiative transitions are represented by solid arrows and non-radiative transitions by arrows with a dashed line.*

All states have different life-times as is reflected by the decay-rates. Decay-rates are referred to as k_{xy}, where x denotes the state from which the transition occurs and y the state into which the molecule ends up (see Fig. 2.1). The lifetime of the lowest vibrational level of the S_1 state is typically on the order of nanoseconds. This is much longer than the lifetime of any of the vibrational levels (picoseconds). The lifetime of the triplet state is rather long (microseconds up to seconds), as the

transition from the triplet state down to the singlet ground state is spin forbidden. During the time a molecule resides in the triplet state, no emission will be observed.

The intensity ratio of the de-excitation lines is determined by the Franck-Condon and the Debye-Waller factors. The Franck-Condon factor is determined by the internal properties of a molecule and takes into account the reduction of the absorption cross-section due to vibrational sub-levels of a molecule. The Debye-Waller factor is a measure for the intensity distribution between the zero-phonon line and the phonon wing, which is determined by the temperature and the properties of the molecule-matrix system. The Debye-Waller factor decreases exponentially with temperature [24].

Since the very beginning of single-molecule detection at low temperature in solids, two techniques have been used: absorption [1] and fluorescence excitation [2] spectroscopy. The coherently scattered light, which has exactly the same wavelength as the excitation light, is detected in absorption experiments. Modulation techniques have been used to detect the signal from single molecules [1, 25–27] although it was shown that single molecules could also be detected in absorption without the use modulation techniques [28]. In fluorescence excitation experiments, the Stokes-shifted fluorescence is detected [2]. Filters are placed in front of the detector to cut the excitation light. This also means that the resonance fluorescence of the molecule is cut and usually, depending on the molecule-matrix system and the filters in use, part of the Stokes-shifted fluorescence as well. Nevertheless, the latter method became more popular as it is easier to perform and detection of single molecules is straightforward.

2.1.2 Getting down to the single-molecule level

One method to get down to the level of single molecules is to reduce the concentration of the impurity molecules. When the concentration is reduced far enough, only one molecule that is in resonance with the excitation frequency is left in the excitation volume. This method is referred to as “spatial selection” and is the only available method for single-molecule experiments at room temperature. Due to the narrow zero-phonon lines of single molecules at low temperature, the concentration at which only one molecule in the excitation volume is in resonance with the incoming laser frequency is far higher at low temperature than at room temperature. The narrow

zero-phonon lines give rise to the additional criterion to address single molecules at low temperature, which is called "spectral selection".

Ensemble spectra consist of relatively broad bands. The width of these bands was found to be smallest for single crystals, intermediate for Shpol'skii systems and broadest for amorphous systems or glasses [23]. In fact these bands are inhomogeneously broadened lines, which are the sums of the homogeneous zero-phonon lines of all single molecules contributing to the bands. Due to the fact that the zero-phonon line is very sensitive to the local environment, a slightly different environment of the guest molecule in the host matrix will result in a slightly different absorption frequency (see Fig. 2.2). This means that the width of these bands reflects the spread in interaction strengths of the impurity molecules with the host molecules in their local environment in the matrix. To apply spectral selection, a laser with a bandwidth narrower than the homogeneous line-width of a single molecule has to be used, such that the molecule goes in and out of resonance on scanning the laser frequency. In the centre of the band, an inhomogeneously broadened line might still be present, depending on the concentration of the sample. When probed with a narrow band laser, the inhomogeneous line is not smooth, but shows narrow spectral features on it. On repeated scanning over the same spectral range, the same features will be found. These narrow spectral features are the signals of single molecules on top of a sum of many single-molecule signals. These narrow resonance lines of single molecules on top of a "background" of many molecules are called "statistical fine-structure" [29]. On tuning to the wings of the band, less and less molecules will be excited simultaneously, until only a single molecule is left. For single molecule experiments on molecules in the centre of the band, the concentration has to be reduced further.

The homogeneous line width of a single molecule is described by [4]:

$$\Delta\nu_{hom} = \frac{1}{\pi T_2} = \frac{1}{2\pi T_1} + \frac{1}{\pi T_2^*} \tag{2.1}$$

where $\Delta\nu_{hom}$ denotes the full width at half maximum (FWHM) of the homogeneous line, T_2 the total dephasing time of the optical transition, T_1 the lifetime of the excited state and T_2^* the pure dephasing time. At low temperature, T_1 is independent of temperature, while T_2^* strongly depends on temperature. The value of T_2^* depends on the excitation of low frequency vibrational modes, like phonons and

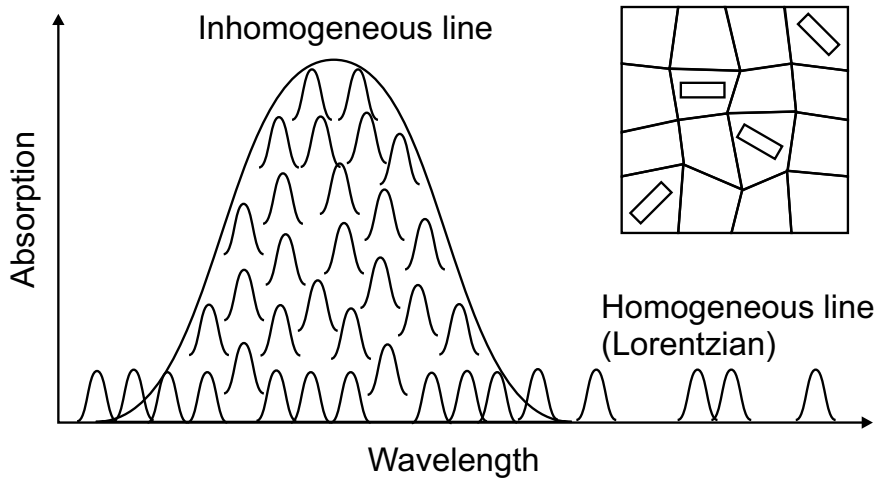

Figure 2.2: *Illustration of an inhomogeneously broadened line and the principle of spectral selection of single molecules in solids at low temperature. The inhomogeneous line is formed by a superposition of homogeneous lines of single molecules. The differences in absorption frequencies of single molecules are caused by differences in their local host environments, as is illustrated in the right-hand top corner. The general structure represents the host matrix and the rectangles the impurity molecules in the matrix.*

librations, that couple to the electronic transition of the impurity molecule. For molecules embedded in single crystals at temperatures below 2 K, T_2^* approaches infinity and the homogeneous line width approaches the lifetime limited value. For molecules embedded in other matrices, like polymers, the homogeneous line width is still broadened at temperatures of about 2 K (see section 5.3.4). The lifetime limited homogeneous line width for impurity molecules in polymers is only reached at significantly lower temperatures [30].

2.1.3 Requirements for the molecule-matrix system

Unfortunately, not every molecule-matrix system is suited for single molecule spectroscopy at cryogenic temperatures. Requirements for the molecule-matrix systems involve both properties of the host and of the guest molecules. The collection efficiency of the experimental set-up also plays an important role.

Single molecules can only be excited if the square of the component of the electric field vector of the excitation light along the transition dipole moment of the

single molecule is larger than 0. The electric field components in the excitation volume depend on the technique: under confocal excitation, the electric field components are mainly in the plane perpendicular to the propagation direction of the light, whereas under near-field excitation, components both parallel and perpendicular to the end-face of the tip are present, with varying amplitudes depending on the position with respect to the aperture [10]. This basically means that molecules in some matrices, oriented almost perpendicular to the sample plane, are not suitable for optical investigations using confocal microscopy, but might be well suited for other techniques, like scanning near-field optical microscopy.

An unfavourable three-dimensional orientation results in a relatively high saturation intensity (e.g. terrylene in *p*-terphenyl [31], compared to terrylene in a stretched film of linear low-density polyethylene [32]) and a reduced absorption cross-section. High saturation intensities are usually not considered problematic, as the laser intensity needed to saturate a single molecule that is oriented unfavourably corresponds to a power on the order of a few μW. The absorption cross-section should preferably be as large as possible to maximise the ratio between the absorption cross-section of the molecule and the excitation spot to facilitate single-molecule detection.

The absorption cross-section denotes the effective photon-capture area of a single molecule under resonant excitation. The mechanism behind it is a near-field effect, caused by the interference of resonantly scattered light and excitation light in the near-field of the absorber. As a single molecule at low temperature doesn't scatter all light resonantly, the absorption cross-section is reduced compared to a perfect two-level system.

The low light intensity resonance cross-section, σ, of a single two-level atom in vacuum including radiation-less energy losses is classically described by [33, 34]:

$$\sigma = \frac{3\lambda^2}{2\pi}\frac{\Gamma^2}{\Gamma_t^2} \tag{2.2}$$

where λ denotes the wavelength, Γ the radiative decay rate and Γ_t the total decay rate. For a molecule doped into a solid matrix with an energy diagram as shown in Fig. 2.1, the absorption cross-section σ is reduced by the Franck-Condon, α_{FC}, and the Debye-Waller, α_{DW}, factors. Further reduction due the angle ϑ between the transition dipole moment of the molecule and the electric field vector of the

excitation light gives rise to an additional factor of $\cos^2\vartheta$. Taking into account all these factors, the absorption cross-section of a single molecule in a solid matrix can be written as:

$$\sigma = \alpha_{FC}\alpha_{DW}\frac{3\lambda^2}{2\pi}\frac{\Gamma^2}{\Gamma_t^2}\cos^2\vartheta \tag{2.3}$$

Typical values of the absorption cross-section, σ, for a molecule at low temperature are on the order of 10^{-10} cm^2 [6] to 10^{-11} cm^2 [4] The main contribution comes from the factor of $3\lambda^2/2\pi$, which for $\lambda = 580$ nm is $1.6 \cdot 10^{-9}$ cm^2. The other factors together thus contribute by a factor of about 0.1. This factor corresponds to the fraction of all decays which the molecule emits as resonance fluorescence. The absorption cross-section at low temperature is far larger than the absorption cross-section of the same single molecule at room temperature, 10^{-17} cm^2, and 10^4 times bigger than the physical size of the molecule itself [6].

The highly increased absorption cross-section of a single molecule at 1.8 K can be explained with a classical picture. The molecule is considered a classical dipole, emitting a dipole field that is characterised by a Lorentzian resonance line shape and a Poynting vector $\mathbf{S}_{\mathrm{SCATTER}}$. The molecule is excited by an incoming plane wave with Poynting vector $\mathbf{S}_{\mathrm{IN}}$. The electric field of the excitation wave is parallel to the transition dipole moment of the molecule. In the near-field of the molecule, the coherent part of the molecular emission interferes with the incoming beam. The total Poynting vector then reads $\mathbf{S}_{\mathrm{TOT}} = \mathbf{S}_{\mathrm{SCATTER}} + \mathbf{S}_{\mathrm{EXT}} + \mathbf{S}_{\mathrm{IN}}$, where $\mathbf{S}_{\mathrm{EXT}}$ is an interaction term [35, 36]. The sum of $\mathbf{S}_{\mathrm{IN}}$ and $\mathbf{S}_{\mathrm{EXT}}$ represents the flow of energy towards the dipole as is plotted in Fig. 2.3A and B for resonant and non-resonant excitation, respectively. The near-field interference effect causes the flow of electromagnetic energy to be directed towards the resonant molecule whereas it mainly passes a non-resonant molecule. The area out of which the electromagnetic energy is collected and directed towards the molecule can be identified with the absorption cross section.

Other desirable properties of the impurity molecule are a low probability that the molecule undergoes a transition to the triplet state and high quantum efficiency. The quantum efficiency is a number between 0 and 1, and is the number of emitted photons divided by the number of absorbed photons. Molecules with high quantum efficiency are not only good absorbers, but also good emitters and thus provide enough signal for detection. Molecules that often undergo intersystem crossing and reside a relatively long time in the triplet state are unfavourable as no light will

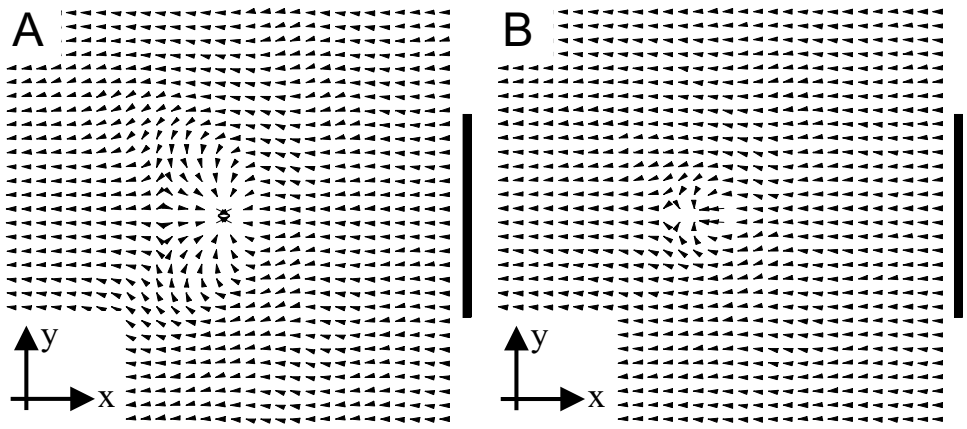

Figure 2.3: *Energy flow (Poynting vector* $\mathbf{S}_{\mathrm{EXT}} + \mathbf{S}_{\mathrm{IN}}$*) towards a dipole (A) in resonance and (B) out of resonance. The scale bars correspond to 1 wavelength.*

be emitted (or absorbed) during this time. This property depends not only on the molecule itself, but also on its environment and can vary for different absorption bands of a molecule in a matrix or crystal (e.g., for the sites of pentacene in *p*-terphenyl [37]).

As far as the matrix is concerned, the matrix material has to be transparent at the excitation and emission wavelengths of the guest molecules under study. It means that the matrix molecules shouldn't interact with light at the excitation or emission frequency of the guest molecules under study. Additionally, the Debye-Waller factor (electron-phonon coupling) should be low, as this determines the amount of line broadening, which also affects the absorption cross-section of the guest molecules. And finally, the combination of host and guest molecules should result in spectrally stable and high intensity single-molecule emission. Some host matrices might be suitable for one guest molecule, but not for others [4, 8]. Single crystals are often stable matrices, as they have a regular, well-defined structure. Impurity molecules in single crystals all have a very similar local environment of matrix molecules. The spread in interaction strengths of the impurity molecules with the matrix is small, as is illustrated by narrow bands in the ensemble spectra [23]. Polymers on the other hand have a very irregular structure, leading to variations in the local environment of the impurity molecules and a spread in interaction strength between impurity molecules and their local environment. Due to the irregular structure of a polymer matrix, dephasing processes lead to a broadening of the line-width at 2 K. The line-

width of an impurity molecule in a polymer matrix only reaches the life-time limited line-width at temperatures well below 2 K [30].

2.1.4 Saturation

Under excitation at low intensities, the number of photons absorbed by a molecule increases linearly with the excitation intensity. When the excitation intensity is increased more and more, saturation starts gradually. When a molecule is fully saturated, it can't absorb more photons when the intensity is increased further. The intensity at which molecules are fully saturated depends on the molecule and its orientation in the matrix. Determination of the saturation parameters is often considered necessary to realize optimised experimental conditions only. In fact, analysis of saturation data requires decent knowledge of the detection efficiency of the whole set up including the collection efficiency of the objective, filters and the detector [38]. Additionally, saturation data provide important information on the three-dimensional orientation of the transition dipole moment of a single molecule, which is obscured in confocal polarisation microscopy [38].

A theoretical description of saturation of single molecules [39] follows the work by De Vries and Wiersma [40], using optical Bloch equations for the elements of the corresponding density matrix. From the steady state solution for a three level system, the following equations for the intensity dependence of the fluorescence emission rate R of a single absorber and of the excitation line-width $\triangle\nu_{FWHM}$ (full width at half maximum) were derived [41]:

$$R(I) = R_\infty \frac{I/I_S}{1 + I/I_S} \tag{2.4}$$

$$\triangle\nu_{FWHM}(I) = \triangle\nu(0)\sqrt{1 + I/I_S} \tag{2.5}$$

where R_∞ denotes the maximum emission rate, I the excitation intensity, I_S the saturation intensity and $\triangle\nu(0)$ homogeneous line-width (the full width at half maximum) at 0 intensity.

Eq. 2.4 describes the effect that the amount of absorbed and emitted photons asymptotically reaches a maximum value under saturation conditions. It demonstrates that under excitation at saturation intensity, $I = I_S$, the emission rate will

be half of the maximum emission rate, R_∞. For even higher excitation intensities, the emission rate will approach asymptotically the maximum emission rate, R_∞.

Eq. 2.5 on the other hand, gives an expression for the effect of spectral broadening of the zero-phonon line. It also shows that the true excitation line-width, $\triangle\nu_{FWHM}(0)$ could only be measured at 0 intensity. In other words, any measured line width of the zero-phonon line will suffer from some power broadening, even under conditions far below saturation.

Another effect of saturation is the reduction of the absorption cross-section, σ (see Eq. 2.3) with intensity [4, 42], according to:

$$\sigma_S = \frac{\sigma}{1 + I/I_S} \tag{2.6}$$

where σ_S denotes the absorption cross-section under saturation, I the excitation intensity and I_S the saturation intensity. The decrease in absorption cross-section can be understood from its physical nature. Under saturation, the coherent part of the emission from a single molecule is decreased. As a result the amount of re-emitted light available for interference is decreased and a reduced amount of interference results in a smaller absorption cross-section. For high intensities the absorption cross-section asymptotically approaches 0.

2.2 Optical imaging and spectroscopy

2.2.1 Resolution

Traditionally, the word resolution was used in optical microscopy according to the Rayleigh criterion to designate the smallest separation needed to distinguish two different objects in a microscope [43]. The meaning of the word resolution has to be checked carefully in every study, as it is also used to designate position determination accuracy. However, even if a position is determined with a sub-diffraction limited accuracy, two objects as close together as the claimed resolution might still not be separated. Throughout this thesis, the word resolution will be used in its classical meaning.

Two types of optical microscopy were used in the experiments described in this thesis: confocal microscopy and aperture scanning near-field optical microscopy. Confocal microscopy is a non-invasive, far-field technique, which allows for imaging objects both close to a surface and deep inside a sample. The resolution is limited by the diffraction limit as formulated by Abbe in 1873 [44]. Aperture scanning near-field optical microscopy is a near-field technique in which the excitation light is provided by a sub-wavelength aperture at the end of a metal-coated tip. The excitation light is highly confined to the aperture and consists of evanescent waves. Aperture scanning near-field optical microscopy can thus be used for experiments on absorbers in the near-field of the aperture tip, which limits its sensitivity to absorbers close to the sample surface. The resolution is beyond the diffraction barrier.

2.2.2 Confocal microscopy

Confocal microscopy is a classical far-field technique with a resolution limited by the diffraction limit. Nevertheless, it's the method of choice in low temperature optical spectroscopy and it has a wide range of applications in molecular biophysics [45,46]. A short description of the main properties will be provided. Further details and variations on this scheme, like the use of a spinning disk for real time, video rate imaging, can be found in references [45, 47].

The main idea of the confocal microscope is to image only a confined volume of the sample at a time. Usually a point-like light-source is used and the detection is limited to the small area in the focus, as illustrated in Fig. 2.4. To achieve this, two important pin-holes are introduced in the experimental configuration: one in the excitation path and one in front of the detector. The excitation pin-hole defines a point light source, which is imaged at the object plane. From the Rayleigh equation, the maximum resolution r_{RESEL} can be estimated from

$$r_{RESEL} = 0.61 \cdot \frac{\lambda}{NA} \tag{2.7}$$

where λ denotes the wavelength of the light and NA the numerical aperture of the objective. The theoretical resolution r_{RESEL} that can thus be obtained with an objective of NA=0.85 at a wavelength of 580 nm is $r_{RESEL} = 416\ nm$.

The collection optics form an image of the illuminated area on the sample on the detection pinhole. The point light source, the illuminated area on the sample and the image on the detection pinhole are all mutually confocal. The detection pin-hole ensures detection of only the area on the sample that is in focus. In practice this means that light coming from out-of-focus areas is mostly blocked, as it is either focussed in front of the pin-hole (object closer to the objective) or behind the pin-hole (object deeper inside the sample). Proper choice of the pinhole also makes sure that dim objects close to bright objects are still imaged correctly. The optimum resolution is obtained when the size of the detection pinhole corresponds to the geometrical size of 1 resel in the sample plane.

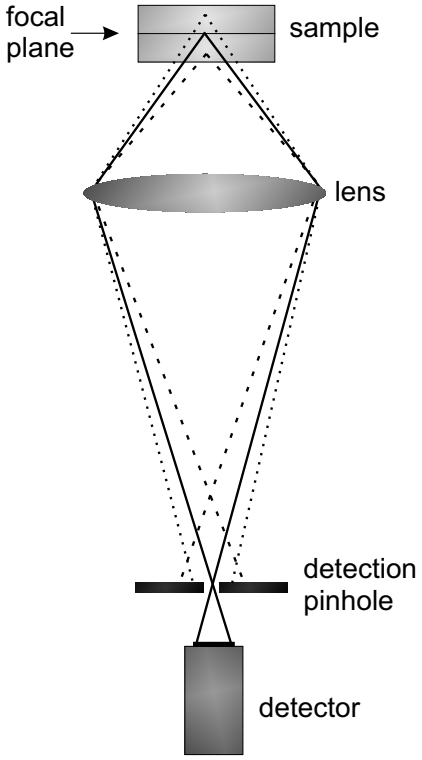

Figure 2.4: *The confocal principle.*

The electric field vector in confocal microscopy under normal illumination only has significant components perpendicular to the propagation direction of the light. This means that in any polarisation experiment, only the projection of the emitter's transition dipole moment on the plane perpendicular to the propagation direction of the light is measured and no information on out-of-plane components is obtained.

2.2.3 Aperture scanning near-field optical microscopy

Aperture scanning near-field optical microscopy with near-field illumination and far-field detection was used in the experiments described in chapter 6. In the following parts, the main features of this scheme will be discussed.

Aperture scanning near-field optical microscopy with near-field illumination and far-field detection uses a sub-wavelength aperture at the end of a metal-coated tip

as a light source [11]. Usual tips are single-tapered etched fibres [48], double-tapered etched fibres [49], or pulled fibres [50]. The metal coating is produced by thermal evaporation or sputtering of a metal, like aluminium [48] or gold [49]. Apertures are created either during the evaporation process, by introducing an angle between the bare tip and the evaporation source [51–53], or by cutting slices from the end-face with a focussed ion beam [54, 55]. Flat end-faces, as produced with the focussed ion beam, offer the advantages of a well-defined aperture and a flat end-face. Due to the grainy structure of the evaporated metal, the aperture is often ill-defined for tips prepared with the shadow evaporation technique. Difficulties arise in the determination of the exact aperture size and the precise aperture-sample distance.

The resolution in aperture scanning near-field optical microscopy is roughly determined by the size of the aperture for aperture-sample distances that are smaller than the radius of the aperture [56]. In practical applications with aperture diameters of about 100 nm, this means that the required tip-sample distances are below 100 nm. A feed-back mechanism is required to control the tip-sample separation. A popular non-optical feed-back mechanism is based on shear-force detection using quartz tuning-forks (see section 3.3.2).

Contrary to confocal optical microscopy, the electric field vector of the light at a sub-wavelength aperture has out-of-plane components [10, 57, 58]. The electric field vector stands perpendicular to the surface at the glass-metal interface and turns to parallel orientation in the centre of the glass-aperture. For well-defined polarisation directions, this property can be exploited to directly image the three-dimensional orientation of the emitter under study.

The polarisation of the light, coming through the aperture tip as observed in the far-field, depends strongly on the quality of the aperture tip. Ideal tips have perfectly flat end-faces and perfectly circular apertures. Such tips show a good symmetry, allowing for circular polarisation, but linear polarisation with a ratio of $1 \div 205$ could also be achieved [55]. However, tips are often not ideal, and show asymmetric aperture shapes. The polarisation of the light coming out of slit-like apertures was predicted theoretically [59] and shown experimentally [60] to be mainly polarised along the short axis of the aperture. Experimental determination of the main polarisation of other aperture shapes can be found in Ref. [60].

3. Experimental

The experimental set up consists of a (home-built) confocal microscope, with a scanning near-field optical microscope on top of it. The experimental arrangement and the full power of the instrument are described. After that, a short description of the preparation of the samples used in this work is provided.

3.1 The optical set up

3.1.1 Overview

A schematic drawing of the optical set up is shown in Fig. 3.1. The light from a single-mode ring dye-laser is coupled into an optical fibre to decouple the adjustment of the confocal set up from any adjustment being made on the laser. After that, the laser power is stabilized (CRI LS-PRO-VIS) and the light can be directed either into a fibre with a SNOM tip at its very end or into the confocal microscope. In the confocal microscope, the beam waist is enlarged using telescopic lenses to overfill the entrance aperture of the microscope objective (Microthek, 0.85 NA, f= 2.9 mm, 60×, (several types)). Before entering the objective, the polarisation is controlled with a quarter-wave plate and a half-wave plate. Then the light is filtered with a narrow band-pass filter with a band width of 1 nm (Omega Optical, 580NB1) and part of the light, which is reflected by a glass wedge (∼4%) mounted at a small angle, is directed into the microscope objective. The microscope objective is inside a helium bath-cryostat and focuses the light onto the sample.

The main part of the light, which is transmitted by the wedge, passes a neutral density filter and is retro-reflected by a mirror on a translation stage. The light is then overlapped again with the incoming beam on the wedge. This light path acts as a second arm of an interferometer and can be used as an external reference beam in absorption experiments. The length of this arm can be varied either by turning the micrometer screw of the translation stage or by applying a high voltage to a piezo (P-171, Physik Instrumente) which is located in the translation stage. This path was blocked during fluorescence excitation measurements.

In both confocal and near-field excitation, fluorescence and backscattered light are collected by the same objective as was used for (confocal) excitation. The light transmitted by the wedge (∼96%) is filtered using a holographic Notch filter (Kaiser Optical Systems, 583 nm). Stokes-shifted fluorescence is transmitted by the Notch filter and focussed by a 300 mm achromatic lens onto a single-photon counting avalanche photodiode (SPAD) (PerkinElmer, SPCM-AQR13). The back-scattered laser light and the resonance fluorescence are reflected by the Notch filter. For absorption experiments, this reflected light is directed on a mirror and focussed by a 1000 mm lens onto a second SPAD. The longer focal length of this lens compared

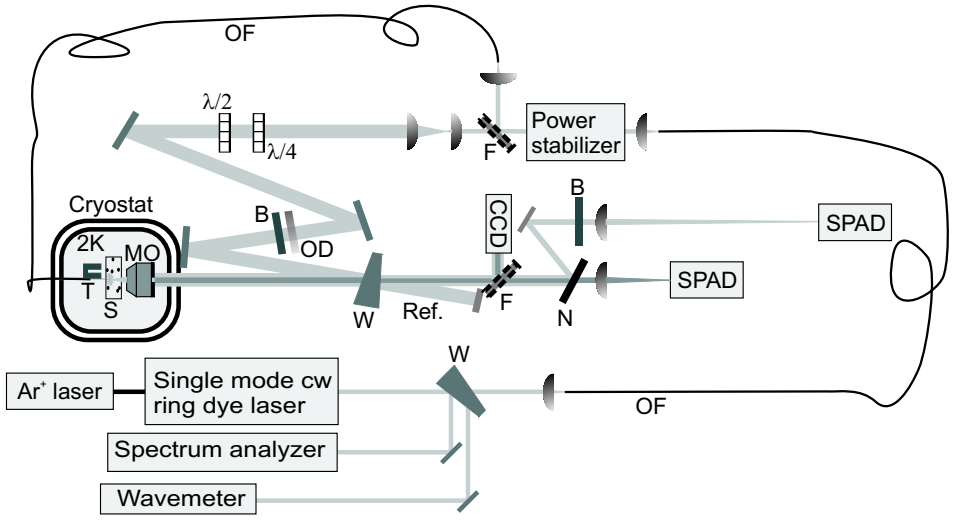

Figure 3.1: *Schematic drawing of the optical set up: (W) glass wedge, (OF) optical fibre, (F) flipping mirror, (OD) wheel with neutral density filters, (B) band-pass filter with a width of 1 nm at 580 nm, (MO) microscope objective, (S) sample, (T) tip glued to a tuning fork, (N) Notch filter, (Ref.) Reference beam in absorption experiment, (SPAD) single photon counting avalanche photodiode and (CCD) charge coupled device camera.*

to the fluorescence path was chosen to cut off a bigger part of the light not coming from the confocal area. The small entrance apertures of the SPADs with a diameter of 200 μm act as detection pinholes. From the focal lengths of the lenses in the detection paths, the size on the detection pinhole corresponding to 1 r_{RESEL} (see section 2.2.2) in the sample can be calculated. For the fluorescence detection path, the size of 1 r_{RESEL} is magnified by a factor of 300 $mm/2.9$ mm. The size on the detection pinhole corresponding to 1 r_{RESEL} is then 43 μm, or a diameter of 86 μm. This is far smaller than the diameter of the entrance aperture of the SPAD, which is 200 μm. In other words, the light from 2.3 resels in the sample is imaged on the SPAD. For the absorption detection path, 1 r_{RESEL} is magnified to a size of 144 μm, or a diameter of 288 μm. The diameter of the detection pinhole is smaller than the geometrical size corresponding to 1 r_{RESEL}. The light coming from 0.7 resel in the sample is detected on the SPAD. The ideal detection area corresponding to 1 resel would be achieved using a lens with a focal length of 697 mm.

For visual inspection of the sample, the light can be directed onto a CCD camera, which is connected to a video screen. The CCD camera is especially useful

for focussing of the light, adjustment of the tip position with respect to the confocal volume and tip approach. Alternatively, it can be used to check tip- or sample-scanner motion.

3.1.2 The laser system

The excitation light is provided by a single-mode ring dye-laser (Coherent 699-21), which is pumped by a multi-line Ar^+-laser (Spectra Physics Model 2045 / Coherent Innova 300, typical output power 4.5–5 W). The dye-laser is operated in single mode with Rhodamine-6G (Radiant Dyes), allowing continuous tuning of the wavelength between roughly ~ 569 nm and ~ 605 nm. Its bandwidth of about 1 MHz is narrower than the typical line width of the chromophores (≥ 50 MHz).

The wavelength can be scanned stably over intervals of up to 25 GHz and is monitored with a wavemeter (Burleigh WA-10, precision 0.003 nm). Stable single-mode operation is verified with a spectrum analyser (Tropel, Model 240). The frequency stability over longer time periods is checked regularly by recording the spectrum of an iodine cell (which is then placed at the position of the wavemeter, see Fig. 3.1). As the iodine spectrum shows many lines and the pattern of the lines changes clearly with excitation frequency, the long-term observation of the spectrum provides a good measure for drift in frequency. Laser drift as specified by the manufacturer was < 100 MHz/hour.

The typical output power from the dye-laser was at least 250 mW. As only a fraction of the light was needed for the experiment, neutral density filters were used to adjust the power. Alternatively, the power from the pump laser was reduced to 4–4.5 W.

3.1.3 The cryostat

The whole experimental stage is sitting inside a home-built helium bath-cryostat. The only window of the cryostat is at the bottom.

The inner part of the cryostat has a relatively large diameter (at least ~ 11 cm) to meet with the requirements of the relatively big experimental stage. The cryostat has several layers for heat protection. From the outside, the first layer is a vacuum

shield, pumped down to a pressure of about 10^{-6} mbar. The second layer is a shield which can be filled with liquid nitrogen. The third layer is again a vacuum shield at the same pressure as the other vacuum shield (actually they are connected), followed by the inner part that is filled with liquid helium.

Liquid helium (^{4}He) is boiling at 4.2 K, and as such not transparent. When pumping on the helium bath, the helium gets superfluid below the Λ-point (T = 2.17 K) and after this phase-transition, the helium is transparent and no longer boiling. Experiments are performed at pressures of about 30 mbar or lower, which is well below the Λ-point. The corresponding temperature at this pressure is slightly below 2 K.

3.2 The confocal experimental stage

The confocal experimental stage is the part of the confocal set up that is located inside the cryostat (see Fig. 3.1 and Fig. 3.2). It consists of a microscope objective, a disc piezo, a sample scanner and three stacks of two shear piezos for coarse sample displacement. In the following, a short description of the main elements is presented. A more detailed description is given in references [61, 62].

The microscope objective can be moved up and down for focussing using a stepper motor (Princeton Research Instruments, size A). The current generated by the power supply (Princeton Research Instruments, SK-1) is attenuated using resistors to guarantee stable operation and to reduce mechanical vibrations introduced by motor movements. The movements of the motor suffer from hysteresis, which limits its use to coarse focussing of the light onto the sample.

Fine focussing is obtained with the disc piezo (Piezo Mechanik, CBM100/35-5/070), which at the same time keeps the sample holder in place. The disc piezo is supported by a thin holder with 3 holes and 3 sapphire plates on the lower side. The disc piezo in its holder is kept in position by 3 NdFeB magnets and rests on 3 sapphire balls that are glued on top of the shear-piezo stacks. It has a circular hole in the centre which is enlarged in diameter in order to exceed the diameter of the microscope objective. The sample holder rests on the rim of this central hole of the disk piezo. The range of the disk piezo (before enlargement of the central hole) is specified to be ± 70 μm at room temperature (corresponding to applied

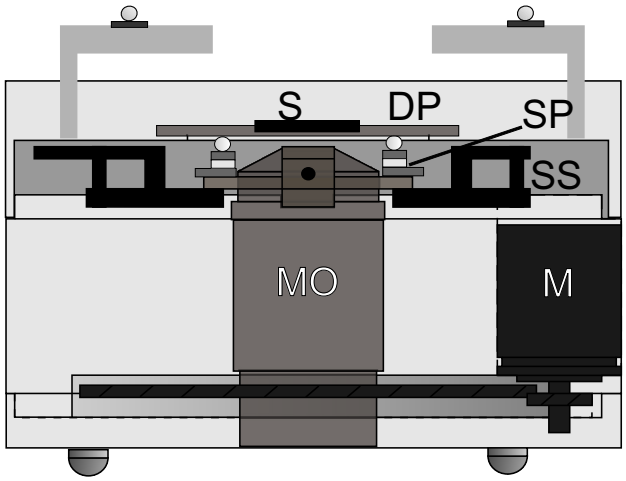

Figure 3.2: *The part of the confocal microscope that resides inside the cryostat: (MO) microscope objective, (M) stepper motor, (S) sample, (DP) disk piezo, (SS) sample scanner and (SP) shear-piezo stack.*

constant voltages between −100 and 100 V). At cryogenic temperatures this range is significantly reduced (roughly by a factor 10 [63]), however a small displacement for focussing can be used.

Sample displacement is obtained with shear-piezo motion. It is implemented to make sure that different areas on the sample can be selected for experiments. Shear piezos (Staveley Sensors Inc., EBL #2 shear mode, 5.0×4.0×1.0 mm) with nickel electrodes on the upper and lower sides of the piezos are used to build stacks. Stacks consist of two shear piezos, which are glued orthogonally on top of each other with a thin macor insulation plate in between. This arrangement allows for movements in 2 orthogonal directions. The lower lying piezos are glued on their lower side to a ring which is fixed to the sample scanner. Fixation of the lower side of a shear piezo results in a relative motion of the upper side compared to the lower side on applying a saw-tooth shaped high-voltage difference between the electrodes of the piezo. When the voltage is built up, the upper side of the piezo moves and the sample holder follows the movement of the piezo (it sticks). When the voltage suddenly drops, the piezo retracts, but the sample holder can't follow the fast motion and stays in its position (it slips). This so-called inertial slip-stick motion is used in many applications, where fine-positioning is needed [64–69]. With the current design, high voltage ramps with a saw-tooth shape with a frequency of 800 Hz and an amplitude of 600 to 1000 V can be applied to both piezos simultaneously. However, in practice, the use of one direction at a time is preferred to reduce the risk of sparks between the two piezos.

The sample scanner is built from four bimorph piezos (Piezo systems Inc., PSI 5H4E, x-poled, 50×5×0.51 mm) [70,71]. Bimorph piezos work as bending actuators

on applied voltages. Two bimorph piezos (which are located opposite to each other) are fixed in position at their centres and the other two bimorph piezos are attached in their centres to the ring with the shear piezos and the disc piezo with the sample holder. On applying the same voltage to two bimorph piezos opposite to each other, a bending is induced, resulting in a movement of the sample. In this way, the sample can be scanned by scanning the voltage-difference to one pair of piezos at a high speed and the voltage difference to the other pair of piezos at a much lower speed. All scanning directions are possible by varying the relative speed with which the voltages going to the piezo pairs are scanned. In its current configuration, the scan range is about $340 \times 340\ \mu\text{m}^2$ at room temperature and about $34 \times 34\ \mu\text{m}^2$ immersed in superfluid helium, as measured from light reflected by a silicon calibration grid. The corresponding voltages that are applied to one of the piezo layers vary between -180 and 180 V, where the other layer of each bimorph piezo is grounded.

All electric connections to piezos were glued with EPO-TEK® E4110. The non-conductive connections (e.g. of sapphire plates and balls) were glued with Araldit® Standard (Ciba-Geigy). Both could stand the huge temperature differences per cooling cycle well.

3.3 The SNOM head

The SNOM head is a separate entity which allows full control over the tip, i.e. the tip approach and retraction, the tip-sample separation and scanning of the tip in (x,y). Positioning the SNOM head (or actually the tip) with respect to the microscope objective is done with stacks of perpendicularly glued shear-piezos, which operate in exactly the same way as those used for sample displacement (see section 3.2). The speed of the motion is reduced due to the higher mass of the SNOM head as compared to the disc piezo with sample.

The tip scanner is connected via a few Kevlar29 threads (Goodfellow, filament diameter 0.017 mm) to a counter weight hanging over two pulleys (see Fig. 3.3). This weight has a slightly higher mass than the tip scanner to balance the influence of gravity. The tip scanner has a (magnetic) steel plate on its back and is attracted to the vertical translation stage with an NdFeB magnet, which is glued onto a screw, allowing adjustment of the force. The tip scanner is moved up and down using slip-

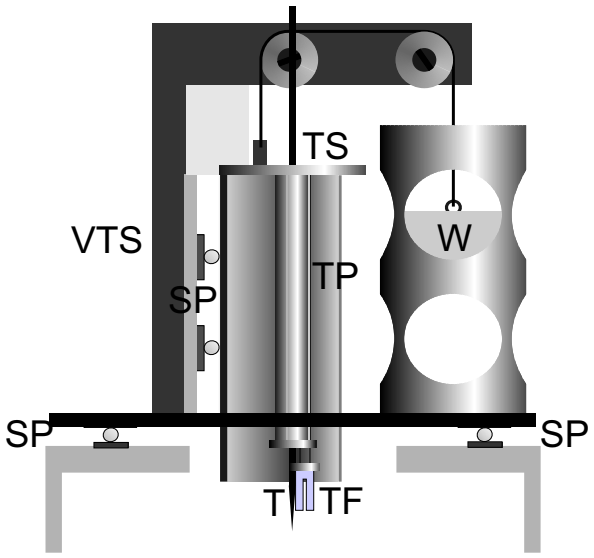

Figure 3.3: *The SNOM head: (TS) tip scanner, (VTS) vertical translation stage, (TP) tube piezo, (TF) tuning fork, (T) tip, (W) counter weight and (SP) shear-piezo stack.*

stick motion induced by four shear-piezo stacks which are mounted vertically. Unlike all other piezo stacks in the set up, these stacks of shear piezos each consist of two shear piezos glued parallel on top of each other with opposite polarisation directions. A conducting layer is between the two shear piezos and a sapphire ball on top. The two shear piezos work simultaneously in the same direction. The doubling of the piezos compared to a previous design [72] was done to facilitate vertical motion of the tip scanner at low temperature. The presence of the magnet is vital for vertical motion as it regulates the attraction of the tip scanner to the vertical translation stage, and the friction force goes linearly with the attraction.

The tip scanner itself has a half-open cylindrical shape. A tube piezo (Staveley Sensors Inc., EBL #2 actuator tube, 3.18×0.51×25.4 mm) is glued in the centre of the top part. The tube piezo is divided into four segments on its outer side and has its fifth electrode on the inner side. A voltage applied to the inner side of the tube piezo causes a change of the length (extension or shrinking) in the vertical direction. Voltages, opposite in sign, applied to two opposite laying outside electrodes result in a bending of the piezo and are used for scanning in the lateral directions.

On the lower side of the tube piezo, a small plate with the quartz tuning fork (ECS-3×8, 32.768 kHz) is connected. The tip is glued to one of the prongs of the tuning fork. The fibre with the tip at its very end is directed through the tube piezo and then connected to a longer fibre which goes out of the cryostat through the top plate. Inside the tube piezo the fibre goes through a heat-shrink to prevent

any unwanted electrical contacts between the metal coating of the tip and the inner electrode of the piezo.

Electrical connections to the tuning fork are made with thin coax cables to provide shielding against interferences due to the voltages applied to the shear-piezo stacks used for the approach mechanism.

3.3.1 Preparation of aperture tips

Single-tapered tips were produced by chemical tube etching of single-mode fibres (3M, FS-SN-3224, cut-off 630 nm), following the procedure outlined in reference [48]. Before etching, the Teflon pot and glass containers needed for tip preparation were cleaned by piranha solution (50% hydrogen peroxide (30%) and 50% sulphuric acid (95-97%)) for 10 minutes. In the mean time, up to 8 fibres of similar lengths were put in a holder. Fibres were fixed in place by a clamping mechanism. Up to 3 cm of fibre was sticking out on the side to be etched. After that, the Teflon pot and the glass containers were rinsed with millipure water. Then, the fibres were put with their holder on the Teflon pot, leaving an opening at the side to fill the Teflon pot with a layer of at least 1 cm of hydrofluoric acid (40%). A thin layer of iso-octane was added on top of it. Tips with a cone angle of about 35° were formed after etching for about 150 minutes. The fibre's polymer coating was only removed after etching by putting the ends of the fibres in hot sulphuric acid or by mechanical stripping. Finally, the tips were put in millipure water to dilute any chemicals remaining on the fibres and to prevent dust deposition. To produce SNOM tips, the chemically etched fibres were placed into an evaporator. At a pressure of $\sim 10^{-6}$ mbar a layer of aluminium was evaporated onto the tips [51–53]. During the whole evaporation process, the tips were rotated to produce a typically at least 300 nm thick uniform layer. Depending on the angle between the rotating tips and the evaporation source, a small aperture could be created at the end of the tips (so-called "shadow evaporation"). For the experiments described in chapter 6, the tips were first coated completely with aluminium. After that, light was coupled into the fibres to make a first check on any tiny holes in the coating. Only tips out of which no light was leaking were used for further processing. These tips were characterised in a scanning electron microscope (SEM) (Philips XL30 FEG). Tips which looked undamaged in the SEM were then cut with a focussed ion beam at

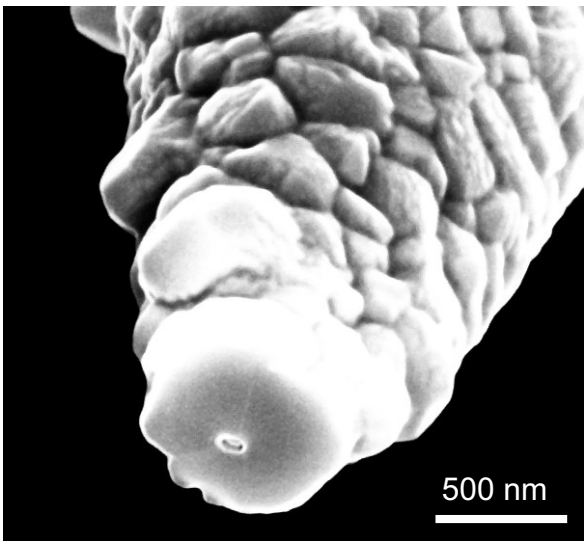

Figure 3.4: *Example of a tip with an aperture of about 100 nm. The aperture was produced by cutting slices from the end of the tip using a focussed ion beam.*

EMPA Dübendorf (Dual Beam FIB, FEI 235). An example of such a tip is shown in Fig. 3.4. With the focussed ion beam, tiny slices of material were cut from the very end of the fibre until an aperture of ideally about 100 nm in diameter was formed [54, 55].

3.3.2 Tip-sample distance control

The tip-sample distance is controlled using quartz tuning forks (ECS-3×8, 32.768 kHz) for non-optical shear-force detection [72–77]. The cap protecting the tuning fork is removed such that only the bare tuning fork remains. The bare tuning fork is fragile, easily damaged and has a reduced quality (Q) factor. The tip is glued to one prong of the tuning fork with a tiny drop of UV glue, such that the tip apex protrudes up to 1 mm. UV glue cures fast under illumination with UV light and is very stiff when cured. Due to the additional mass of the fibre, the resonance frequency of the tuning forks shifts to lower values. Gluing is used despite the disadvantages of the gluing process, e.g. the fact that the tip can't be taken off the tuning fork without damaging the tip (and the tuning fork), and the strong reduction of the Q factor, because methods without gluing usually need more space for the clamping mechanism of the tip to the tuning fork and have a higher mass [78–80]. Higher mass of the tip scanner is unfavourable for approach and retraction at superfluid helium temperatures and space is highly limited.

The principle of shear-force distance control is based on the fact that the resonance frequency of a mechanically excited tuning fork with a tip glued to one of the prongs shifts close to a surface. Theoretical descriptions use a harmonic oscillator model [74] with a driving force and a damping term.

The tuning fork is excited electrically by a sine voltage from a function generator (Yokogawa FG320) at the resonance frequency of the tuning fork with tip. This results in a lateral oscillation of the prongs of the tuning fork. The prongs move in opposite directions. The amplitude of the oscillation depends on the applied voltage. The response of the tuning fork is measured with a lock-in amplifier, using the excitation frequency as a reference signal. A decrease of the tip-sample distance results in a shift of the resonance frequency and phase and a decrease of the amplitude, while the width increases. The feedback mechanism uses the change in amplitude of the tuning fork response as a measure for a change in tip-sample distance.

During approach, first the tube piezo is extended. When no changes in the amplitude of the tuning-fork signal are detected, the tube piezo retracts, and the whole tip scanner is moved downwards by applying a voltage to the stack piezos of the vertical translation stage (see Fig. 3.3). The step made with the vertical translation stage is necessarily smaller than the range of the tube piezo, to prevent crashes during the approach. At the new tip-sample distance, the tube piezo is gradually extended while monitoring the tuning fork signal. If the change in amplitude, when the tube piezo is fully extended, is smaller than the change in amplitude defined as a set point for the feedback loop, the tube piezo retracts again and a next step with the vertical translation stage is made. This cycle is repeated until shear-force contact occurs. Then the feedback loop takes over to assure constant tip-sample distance.

3.3.3 Topographical imaging

The high reliability and accuracy of shear-force detection for tip-sample distance control also permits the use of shear force for topographical imaging purposes. At low temperature, shear-force imaging of calibration patterns was demonstrated both in helium gas [75,77] and immersed in superfluid helium [72]. For this reason, shear-

force detection and imaging of a calibration pattern was only performed at room temperature.

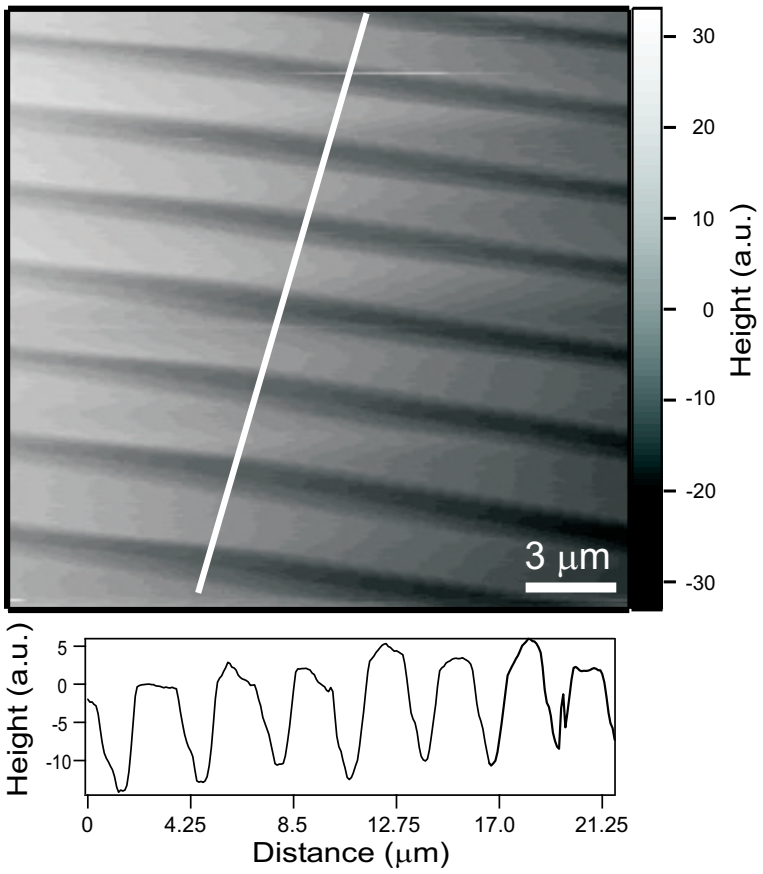

Figure 3.5: *Shear-force image of a silicon calibration sample with a constant period of 3 μm and a depth of 104.5 nm. A line cut along the white line in the image is shown in the lower part of the figure. Heights are given in arbitrary units because the tube piezo had not been calibrated for height determination.*

Shear-force topographical imaging with the improved SNOM head was tested on a silicon calibration grid (NT-MDT, TGZ02) with a period of 3 μm and a step height of 104.5 nm. For shear-force imaging test purposes, only the last cm of an etched fibre was glued to one prong of the tuning fork. Due to the additional mass, the resonance frequency was shifted to a lower frequency. The tip was approached to the sample until shear-force contact occurred. Scanning of the tip with respect to the sample was achieved by scanning the voltages that were applied to the tube piezo. A non-linearity of the tube-piezo response with voltage results in a smaller extension at high voltages than would be expected from a linear behaviour of extension as a function of applied voltage. This non-linearity is observed in the image, which shows a pronounced deformation of the regular calibration structure far away from the centre (see Fig. 3.5). This effect would have been absent if the sample scanner would have been used to scan the tip with respect to the sample, while the tube piezo would only have regulated the tip-sample distance.

3.4 Samples

Two different samples were used for low temperature experiments: single crystals of terrylene in *p*-terphenyl and terrylene in a stretched film of linear low-density polyethylene (LLDPE). The properties of the samples will be described in chapters 6 and 5, respectively. Single crystals of terrylene in *p*-terphenyl have been used in many single-molecule experiments and the sample structure and characteristics can be found in the literature [31, 81, 82]. In chapter 6, the quality of the crystals is discussed in conjunction with the experimental results. For terrylene in a stretched film of linear low-density polyethylene, the situation is different. These films represent a new system for single-molecule spectroscopy at low temperature and needed to be characterised before use. The properties of these films are discussed in chapter 5. A comparison with traditionally pressed samples of terrylene in polyethylene [83–86] is presented as well. The sample preparation will be described in the next section.

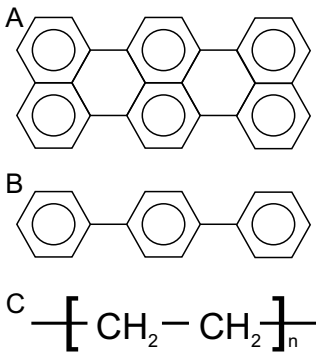

Figure 3.6: *Structures of the molecules. (A) Terrylene, (B) p-terphenyl, (C) LLDPE*

3.5 Sample preparation

3.5.1 Terrylene in *p*-terphenyl

Crystalline platelets of terrylene in *p*-terphenyl were grown in a co-sublimation process [81]. A drawing of the apparatus is shown in Fig. 3.7. A mixture of about 2.5 g *p*-terphenyl (Fluka, used as received) and a few black dots of terrylene (W. Schmidt, PAH Research Institute, Greifenberg (Germany)) were first melted in an oil bath at about 220°C under nitrogen atmosphere, to create a homogeneous base crystal. This resulted in a pinkish melt, which had a darker colour for higher concentrations of terrylene. After letting the base crystal cool down and solidification,

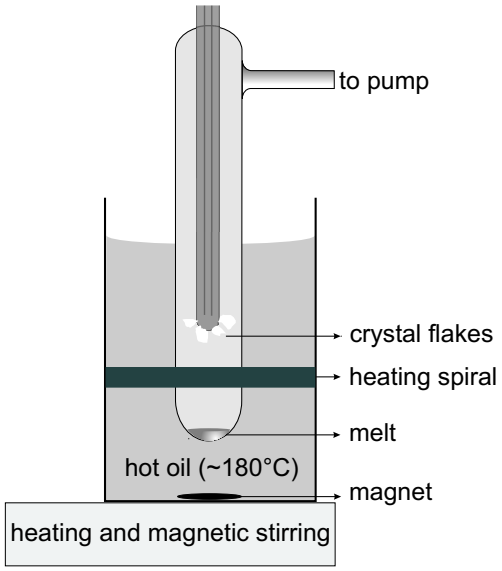

Figure 3.7: *The co-sublimation set up.*

the base crystal was pulverised and put back into the sublimation receptacle. Then, a "cold" finger, filled with a mixture of ethylene glycol and distilled water as a circulating liquid, was heated to about 110°C, while the oil bath was kept at 180°C. The sublimation receptacle was filled with nitrogen gas and pumped out to a pressure of about 40 mbar. Under these conditions co-sublimation started. The process was usually terminated before the cold finger was fully overgrown with crystalline platelets. For experiments, crystalline platelets of several mm in lateral dimensions and about 10 μm thickness were used. These crystalline platelets all stuck to the glass slide by van der Waals interactions. This could eventually cause some additional strain in the crystals, leading to defects.

3.5.2 Terrylene in linear low-density polyethylene

Commercial grade linear LLDPE containing 1.2% octene as a co-monomer was received from the Dow Chemical Company (Dowlex BG 2340, ρ=0.942 g/cm^3). A binary blend of LLDPE and terrylene (40 μg dye/g polymer) was prepared by feeding 100 μg of terrylene and 2.5 g of LLDPE into a recycling, co-rotating twin-screw mini-extruder (DACA Instruments, Santa Barbara, CA), mixing for 5 min at 180°C, and subsequent extrusion. A second blend comprising 1 μg dye/g polymer was subsequently prepared by combining 62.5 mg of the 40 μg dye/g polymer blend with 2.44 g of neat LLDPE and extruding the material in the same manner. Films were prepared by compression-moulding the blends between two aluminium foils, using four spacers, in a Carver press at 180°C for 4 min. Samples were subsequently cooled to about 15°C between water-cooled plates. The resulting films had a homogeneous thickness of about 250 μm. Films were cut to 1 cm widths and uniaxially stretched at 90°C to a draw ratio $\lambda = (l\text{-}l_0)/l_0 = 10$ as measured by the displacement of ink marks on the samples.

4. Single-molecule imaging

Hardly any study so far shed light on the imaging properties of single molecules at low temperature. This chapter presents the results of an experiment in which the same molecule was imaged at different excitation frequencies. Series of images were recorded during which the excitation frequency was slightly changed after each image. Additionally, the experiment was repeated at different excitation intensities. On the basis of results from a Monte Carlo simulation, the observed changes in spot-size could be ascribed to pronounced saturation effects influencing the observed spot of a single molecule in a confocal microscopy image.

4.1 Imaging of single molecules

Most experiments reported so far in the literature on single molecules at low temperatures exclusively exploited spectral selection to address single molecules. Spectrally selective imaging was mainly used to provide information on the axial position of the molecule in the sample and to determine the lateral position of the molecule with a sub-diffraction limited accuracy [17–19]. In these studies the axial position of the molecules was ascribed to the position at which the size of the spot in the image was minimised, resulting in an optimum focus. The lateral positions were determined by calculating the exact centre of the photon distribution with sub-pixel accuracy. Position determination accuracy is also applied in many experiments at room temperature like in biophysics [21, 22].

In contrast to these studies, the experiment described in this chapter deals with single molecules imaged as a function of detuning and intensity, to learn about the properties of single molecules that can be determined by imaging only. Similarly, widths are calculated with sub-pixel accuracy. Experimental results are compared to Monte Carlo simulations that address the spot-size as a function of detuning (i.e. signal-to-background ratio) and the influence of saturation on the spot size. Pronounced saturation effects appear in the experimental data. It turns out that from two high quality images with molecules showing hardly any blinking, one in resonance and one out of resonance, the saturation intensity of the molecule can be deduced. Practically, this method would be much faster than the repeated frequency scanning over the molecule while recording the fluorescence excitation signal.

4.2 Experiment

The properties of single molecules in microscopy images were investigated as a function of detuning and intensity. The experiments were performed on single terrylene molecules in the O_2 site of a crystalline p-terphenyl host. Molecules in this site are standing almost perpendicular to the sample plane in high quality crystals [81, 82] and thus have a high saturation intensity [31, 38]. Defects were clearly present in the crystals under study (see chapter 6 or [87]), which led to molecules having a different orientation. Due to the lower saturation intensity of these molecules and

the higher detected emission rate [38], a bias towards performing measurements on molecules located at a defect site exists.

A typical experiment was performed in the following way: first, a larger sample scan was recorded to localize a single molecule that appeared isolated in space. After that, a high resolution sample scan with a smaller scan-range was recorded centred on this molecule. Typically, the resolution of the scan was adjusted such that a molecule would have a half width at half maximum of about 5 pixels in the image. After precise focussing on the molecule, the frequency was changed in steps of 20 to 40 MHz and after each change in frequency, the molecule was imaged again. At frequencies far out of resonance, no signal from the molecule was recorded any more. At this point, the whole experiment actually really started. From this point onwards, images were recorded again and after each image, the frequency was changed in steps of 10 or 20 MHz until images covering the whole resonance line had been recorded. Additionally for some molecules the intensity was increased after such a series of images and all images were recorded again at a different intensity. As such experiments require stable molecules that can be observed over several hours and long measurement time, only a few molecules could be followed at several intensities.

After locating a molecule and focusing precisely, the focus was kept constant through the whole series of images. This excludes influences on the spot size of a molecule due to a change in focus.

4.3 Results

Images thus recorded were analysed by fitting to two-dimensional Gaussian functions using Igor Pro (Wavemetrics). The widths of the spots in x and y were determined separately as the scan sizes in x and y were slightly different, resulting in asymmetric spots. The fit values for the amplitude and for the half width at half maximum in x and y were used for further analysis.

Some molecules could be imaged over long times at many different intensities. For one such molecule, the saturation behaviour was investigated in detail. The amplitudes that were determined from fitting the spots with a Gaussian were plotted as a function of detuning for each intensity. The result is a fluorescence excitation

line of the molecule as a function of intensity, similar to what would have been expected for a laser scan over a small frequency range around the resonance of the molecule. The spectral line was fitted with a Lorentzian. The amplitude of the Lorentzian, which designates the emission rate per integration time was then plotted as a function of intensity to determine the saturation intensity. The resulting saturation curve is shown in Fig. 4.1. It basically says that the first series of images was taken at the onset of saturation, whereas the other series were taken (far) above saturation.

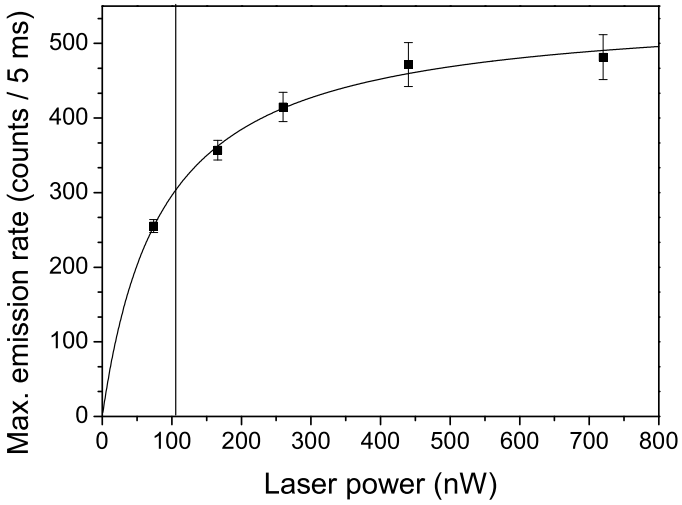

Figure 4.1: *Saturation curve of a molecule of which series of images were recorded at 5 different intensities. The vertical line indicates the laser power at which the molecule was saturated. The indicated laser power was measured at the position where the light enters the cryostat and has not been corrected for any losses.*

The raw data of this particular molecule is summarised in Fig. 4.2. On horizontal lines, five images of the molecule per intensity at different detuning are shown. Note that the changes in detuning between two images are not always as big. On vertical lines, the images at constant detuning but varying relative intensities are shown. The feature that is present in all images at the left-hand top corner stems from a different, near-by molecule, which was not observed in the first scan images of the molecule (not shown). Note the increased occurrence of blinking at higher intensities.

From this data-set, an increase of the spot size with intensity can be inferred. Besides, an increase of the spot size of the molecule in resonance compared to the out-of-resonance size seems to exist. Both effects are pronounced in the fit results. As examples of the change in spot size as a function of excitation frequency, the fit values with uncertainties for the lowest and highest intensities are plotted in Fig. 4.3B. The black circles denote the measured spot sizes at a relative intensity of $0.7 \cdot I_S$ and the grey triangles at a relative intensity of $6.9 \cdot I_S$. A clear increase in the change of spot size under strong saturation is observed.

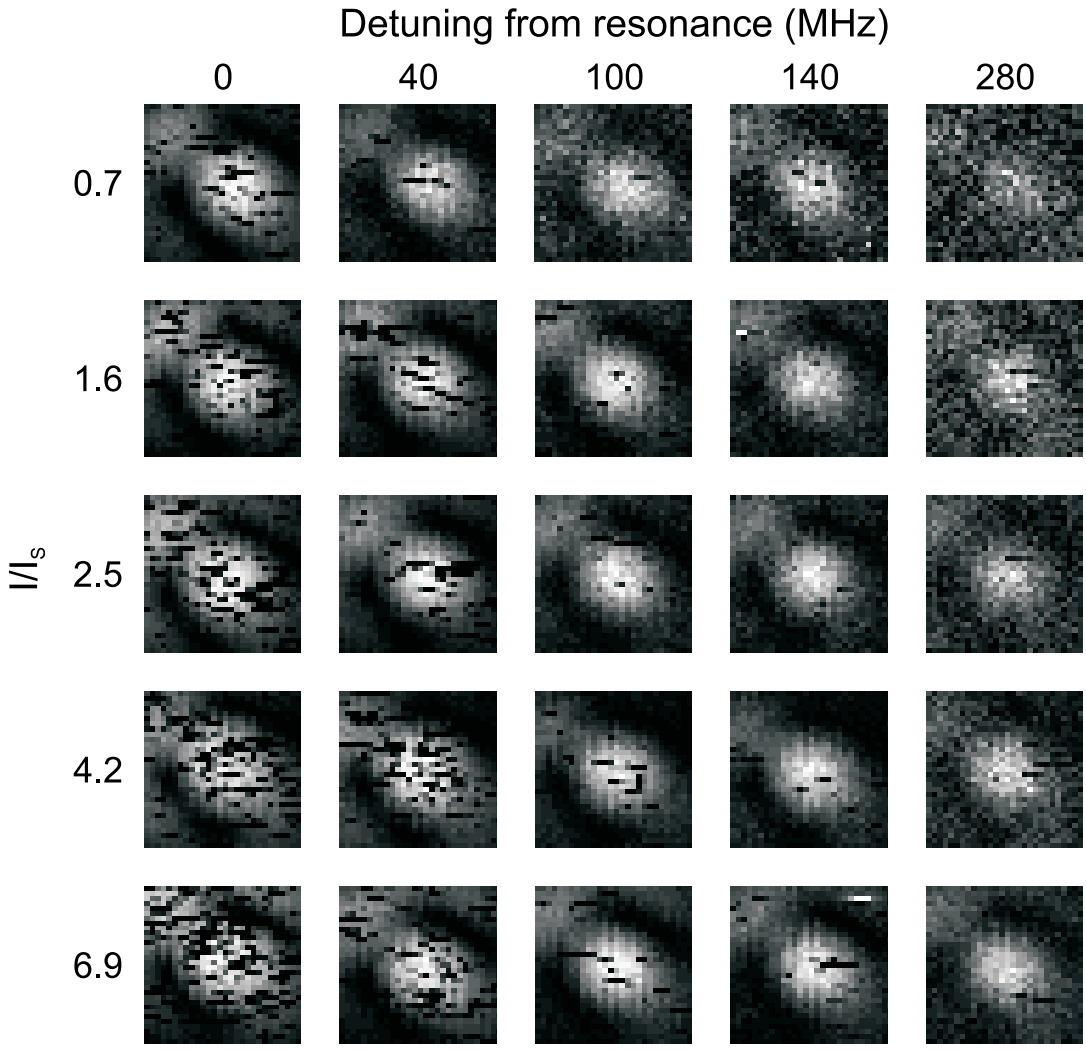

Figure 4.2: *Images of a single molecule as a function of detuning (horizontal axis) and intensity (vertical axis). The spot size increases when the frequency comes closer to the resonance (detuning 0 MHz), or when the intensity is increased. The colour scale of the images is normalized for each image. The size of the images is 1.3 × 1.3 μm^2. The integration time was 5 ms/pixel.*

The spot size in resonance as a function of relative excitation intensity is shown in Fig. 4.3C. An increase in spot size is observed. The uncertainty on the half width at half maximum increases with intensity and is caused by the increased amount of blinking in the spots at higher intensities.

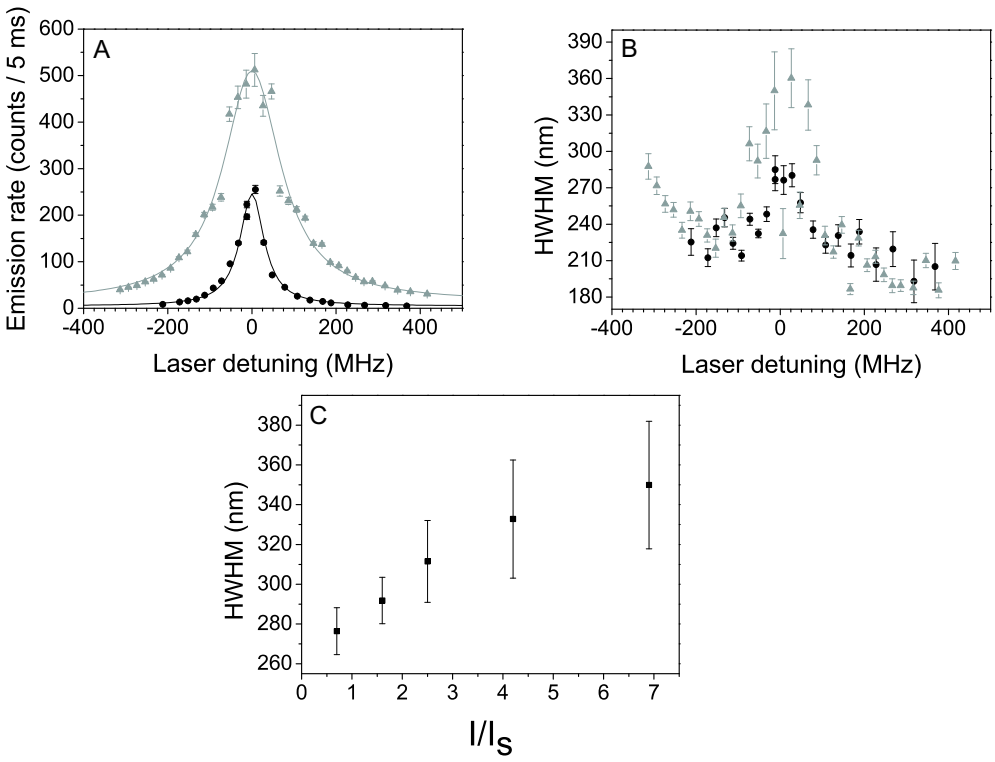

Figure 4.3: *(A) Spectral lines of a single molecule at two different intensities. (B) Corresponding change in the observed HWHM of the imaged spot of the molecule as a function of detuning. The black circles denote the values for $I = 0.7 \cdot I_S$ and the grey triangles for $I = 6.9 \cdot I_S$. (C) HWHM in resonance as a function of relative intensity.*

However, not all molecules show a similar effect. Some molecules don't show any measurable effect in the spot size as a function of frequency even at the excitation intensity that corresponds to the saturation intensity of the molecule shown in this section. Unfortunately, the saturation intensity was not measured for all molecules under study. The molecules that show no effect or a significantly smaller effect at the same intensity are expected to be excited at an intensity far below their saturation intensity. Molecules with higher saturation intensity than other molecules are expected to have a larger angle between the transition dipole moment and the incoming electric field than the molecules with a low saturation intensity [38]. In

this experiment, the light was circularly polarised, meaning that a variation in the angle between the transition dipole moment of a molecule and the incoming electric field is a variation in the orientation of the out-of-plane component of the transition dipole moment. This can be explained by the observed presence of defects in the crystals [87] and the bias towards performing the experiment on molecules at defects. Indeed, many molecules that didn't show any effect as a function of frequency had a five times lower emission rate at the intensity corresponding to $I = 0.7 \cdot I_S$ of the molecule shown in this section.

4.4 Monte Carlo simulations

To gain insight in the accuracy of the determination of the spot sizes of single molecules and to estimate the influence of saturation on the observed spot sizes, Monte Carlo simulations were performed. The main idea behind Monte Carlo simulations is [88] that a statistical method, based on the use of random numbers, is employed to study (physical) problems without the need of complicated theories to describe them. In many cases the use of pseudo-random numbers, i.e. apparently uncorrelated numbers with a pre-defined distribution, may be preferred. In the Monte Carlo simulations described in this section, pseudo-random numbers with a Poisson distribution were used to simulate the noise on the measurements.

The simulations can be split into two parts: the first simulation addresses the question whether a spot with a fixed size is always observed to have this size, even when the detuning increases and thus the signal-to-background ratio decreases. The second simulation addresses the observed change in spot-size under increasing excitation intensities, to determine the influence of the amount of saturation on an observed spot size. Both simulations were run in Mathematica 4 (Wolfram research).

4.4.1 Spot-size as a function of detuning

Whether a change in the measured spot-size as a function of detuning occurs due to the fitting of the spot with a Gaussian function or not was investigated in the first simulation. The simulation addresses this question in a negative testing scheme, i.e. a constant spot size is used. Detuning from resonance results in a decreased

signal-to-background level. The main question is whether this has any influence on the spot-size as determined by the fitting procedure and thus produces the effects that were observed in the experiment.

The spectrum of a single molecule is a homogeneous line with a Lorentzian shape and describes the detected emission rate per integration time R_1 as a function of detuning f:

$$R_1(f) = R_0 + \frac{H}{4 \cdot \frac{(f-f_0)^2}{W^2} + 1} \tag{4.1}$$

where R_0 is the off-set of the background level from 0, H the amplitude, f_0 the resonance frequency and W the Full Width at Half Maximum. As input values, $R_0 =$ 0 counts per integration time, $H = 200$ counts per integration time, $f_0 = 0$ MHz and $W = 60$ MHz were chosen, which represent realistic values from the experiment. The choice of f_0 is actually arbitrary, as a change in resonance frequency results in a shift of the whole curve.

In microscopy images, the molecule is seen as a Gaussian spot, reflecting the shape of the point spread function of the excitation spot. This spot, as a function of position, detuning and size, assuming the spot to be located at (0,0), is given by:

$$spot(x, y, f, \xi) = R_1(f) \cdot e^{-\frac{x^2+y^2}{\xi^2}} \tag{4.2}$$

where x and y denote the $x-$ and $y-$coordinates, respectively, and ξ is a measure for the half width at half maximum (HWHM) of the spot (precisely, $HWHM = \sqrt{\ln 2} \cdot \xi = 0.8326 \cdot \xi$). ξ was set to 5 pixels in all simulations. $R_1(f)$ was defined in Eq. 4.1 and takes the spectral dependence of the amplitude of the spot into account. The function $spot(x, y, f, \xi)$ defines an ideal spot without noise on zero background. Real data has noise and a noisy background. The signal noise is described by a Poisson distribution, which has as mean (μ) and variance (σ^2) the signal amplitude [88, 89]. The background is defined as a low intensity signal with mean 8 with Poisson distribution. As a result, each time the program is run, the spot and background will look slightly different. This is exploited to do predictions on the distributions of the values under study.

Exploiting the symmetry of the problem around f_0, only positive values of the detuning were used in the simulation. For each of 8 different spectral positions studied, 1000 spots were generated. Each spot was fitted with the following Gaussian

function:

$$fit(x, y) = a + b \cdot e^{-\frac{x^2+y^2}{c^2}} \tag{4.3}$$

where the parameter a represents the background level, b the amplitude of the spot and c a measure for the half width at half maximum of the spot in exactly the same way as ξ. From Eq. 4.3 it is obvious that centre positions of the spot that are different from the origin are not considered. Initially this was taken into account by two additional parameters, however, due to the extremely small values (on the order of 10^{-3} to 10^{-4}) that resulted from a first run of the simulation and the huge increase of calculation time, this was omitted in further runs of the simulation.

The thus generated fitting results of 1000 spots per detuning were used to build distributions of the amplitude, b, and the width, c, as a function of detuning. The distributions of the amplitudes with corresponding uncertainties were used to check whether the input was reproduced, as is shown in Fig. 4.4A. The solid grey line represents the input as defined by Eq. 4.1, whereas the dots with error bars show the amplitudes with corresponding standard deviations that came out of the simulation. A good agreement is found.

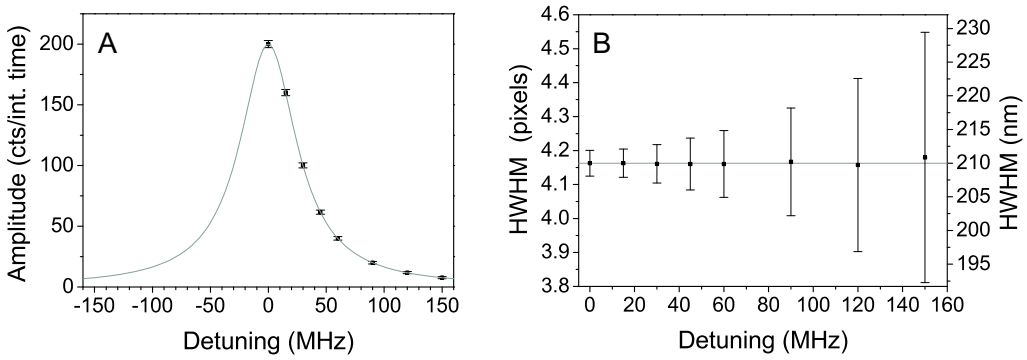

Figure 4.4: *Results of the Monte Carlo simulation on the spot-size as a function of detuning below saturation. (A) The average amplitudes with corresponding uncertainties as a function of detuning (squares) and the input values (grey line). (B) The influence of detuning on the HWHM, both absolute in pixels (left axis), with the corresponding input value as a grey line, and in nm assuming a diffraction limited spot size.*

The distributions of the widths and corresponding uncertainties constitute the main result of the simulation and answer the question whether an observed change in spot size is an artefact from the fitting procedure or not. The distributions of widths at each detuning are shown in Fig. 4.4B. It shows the half width at half

maximum as a function of detuning as dots with corresponding error bars and the input value, $HWHM = \sqrt{\ln 2} \cdot \xi = 4.16$ pixels, as a solid grey line. It demonstrates that at larger detuning, meaning lower signal-to-background ratio, the uncertainties on the widths increase strongly, while the mean value remains extremely close to the input value. The influence of any systematic fitting artefact can be excluded due to the fact that the points are uniformly distributed around the input value. For comparison, the largest deviation from the input value is about 0.02 pixels, which would amount to less than 1 nm for a diffraction limited spot. This means that a constant spot size as input is reproduced in the fitting process with high accuracy and that any increase in spot size observed experimentally at resonance is caused by a physical process. The large error bar of $\sim$ 15 nm at a detuning of 150 MHz indicates that for lower signal-to-background ratio, i.e. in the wing of the line, the uncertainty on the values increases.

4.4.2 Spot-size as a function of intensity

The second simulation addresses the influence of saturation on the observed spot size of a single molecule as seen in the microscope. The molecule was assumed to be excited in resonance at different intensities. Spots were generated by a modification to Eq. 2.4, which describes the emission rate as a function of intensity. The detected emission rate in an image is highest in the centre of the spot and decreases along the Gaussian profile of the point spread function of the excitation spot. The spatial dependence of the emission rate was taken into account by modifying the intensity from a fixed to a spatially dependent variable R_2:

$$R_2(x, y, \zeta) = R_\infty \cdot \frac{\zeta \cdot e^{-\frac{x^2+y^2}{\xi^2}}}{1 + \zeta \cdot e^{-\frac{x^2+y^2}{\xi^2}}} \tag{4.4}$$

In this equation, R_∞ denotes the maximum emission rate and $\zeta = I/I_S$ the relative intensity as a fraction of the saturation intensity. x, y, and ξ are the same parameters as in section 4.4.1. Again, noise with a Poisson distribution was defined both on the spot and on a constant background to get a situation closer to real data. The background noise-level was chosen to have mean 15 counts per integration time, R_∞ was 275 counts per integration time and the width, ξ, was again put to 5 pixels.

For each of 8 different values of ζ, 1000 spots were generated and fitted with the Gaussian defined in Eq. 4.3.

The distributions of the fitting parameters of the amplitude and the HWHM were again plotted to determine mean and standard deviation at each relative intensity. The amplitude was used to check whether the input values were reproduced. The results are shown in Fig. 4.5A. The solid grey line denotes the input, whereas the dots with error bars denote the results from fitting. The black line is a fit with Eq. 2.4 to the data points from the simulation. According to the fit, the maximum emission rate, R_∞ is higher than the input value (330 instead of 275 counts per integration time) and the saturation intensity I_S is a factor of 1.22 bigger. The amplitudes obtained from the fits deviate more and more as a function of intensity. Similarly, the spots also deviate from Gaussians under increasing intensity, as they get flattened on top.

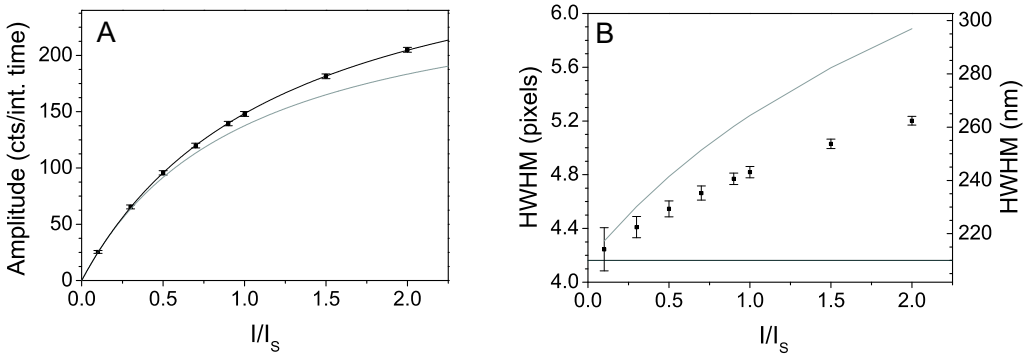

Figure 4.5: *Results of the Monte Carlo simulation on the spot-size as a function of intensity. (A) The average amplitudes with corresponding uncertainties as a function of relative intensity (squares) and the input values (grey line). A fit to the average amplitudes with Eq. 2.4 (black line) shows that the saturation intensity corresponding to the fitted amplitudes is a factor of 1.22 higher than the input. (B) The influence of the excitation intensity on the HWHM, both absolute in pixels (left axis) and in nm assuming a diffraction limited spot size. The vertical line at 4.16 pixels shows the HWHM without any influences of saturation. The grey line shows the calculated HWHM from the input function (Eq. 4.4). A clear increase in spot size as a function of intensity is observed.*

The influence of intensity on the measured HWHM of the spot is summarised in Fig. 4.5B. The grey line indicates the input of the HWHM as calculated from Eq. 4.4, taking into account the effects of saturation. The input value, which doesn't take into account saturation, has a fixed size of 4.16 pixels and is shown as a horizontal

line (dark grey line). The results from the fitting procedure are again represented by dots with corresponding error bars. The HWHM from the fitting procedure clearly underestimates the input. It is obvious that saturation has a large influence on the observed spot size, similar to its influence on the line width. The measured spot size increases even for low intensities clearly below saturation, which means that pronounced effects can be expected in the experimental results.

The fact that the amplitude of the spots is overestimated by the fitting procedure, while the HWHM is underestimated can be explained from the shape of the spot. The generated spots, which take into account the influences of saturation, are flattened on top and become broader when the intensity is increased. These spots thus deviate more from Gaussian spots at increasing intensity. The fitting procedure, however, assumes that the spots can be described by Gaussians. The resulting fits try to minimise the deviations between the data and the Gaussians, resulting in an overestimation of the amplitude and an underestimation of the HWHM.

In this last simulation, one important point was not taken into account, which is the effect of blinking. Under saturation the amount of blinking per image increases heavily. This random event was not included in the generated spots.

4.5 Discussion

The first Monte Carlo simulation (Fig. 4.4B) shows that a decrease in signal-to-background ratio leads to an increased uncertainty on the measured spot size, while the spot size itself stays close to the input value. In the experimental results (Fig. 4.3), a larger spot is found in resonance (highest signal-to-background ratio). This is a clearly different behaviour from what would be expected for a constant spot size and thus can't be classified as a fitting artefact. The pronounced increase in spot size for large negative detuning at $I = 6.9 \cdot I_S$ can be explained as the predicted higher inaccuracy at decreased signal-to-background ratios. The same holds for the small spot sizes at large positive detuning for both intensities, which are smaller than the diffraction limited spot size.

The second Monte Carlo simulation (Fig. 4.5B) shows that the saturation effects in imaging are highly pronounced and lead to increased spot sizes. It also shows that the saturation analysis from the amplitudes of Gaussians fitted to the

spots leads to an overestimation of the saturation intensity, while the width is underestimated. These deviations are due to the fact that the spot of a single molecule under saturation becomes broader and is flattened on top.

The increase in spot size as observed in the experiment agrees within the uncertainty on the data to the predicted change in spot size due to saturation from the second Monte Carlo simulation. The high amount of blinking on the experimental data make the fitting of the spots with Gaussians even more inaccurate. It is thus impossible to correct for the true saturation intensity with the help of Fig. 4.5A. For very good data, showing little blinking, an iterative process could be used to find the true saturation intensity, or alternatively, all images could be fitted with Eq. 4.4. The latter would take into account the flattening of the spot under saturation.

4.6 Conclusion

Saturation effects in the images of single molecules are at least as pronounced as in the line width in single-molecule spectroscopy. A molecule that is imaged under saturation conditions shows a larger spot size than it would show under non-saturating conditions or when imaged far out of resonance. This finding is supported by the results of Monte Carlo simulations. The effect could be exploited to determine whether a molecule is imaged under saturation conditions or not by recording one image in resonance and one image out of resonance and comparing the fitted sizes of the spots. This procedure would be less time consuming than the usual measurements employing spectral scans of the saturation behaviour of a single molecule.

5. Single-molecule detection by absorption

Direct detection of single molecules by absorption remains one of the most challenging experiments in low-temperature single-molecule spectroscopy. The main difficulty resides in the fact that the excitation and emission have exactly the same wavelength and thus can't be separated spectrally. This chapter starts with the specific requirements for the molecule-matrix system for absorption experiments and describes the properties of the ideal sample. A new sample for single-molecule spectroscopy at low temperature, terrylene in a stretched film of linear low-density polyethylene, is characterised. The orientation of the guest molecules in the film makes this sample a particularly good candidate for absorption experiments. Finally, the simultaneous detection of absorption and fluorescence of single molecules using an interferometric method is demonstrated.

5.1 Introduction

Measuring the absorption of light passing through an unknown sample as a function of wavelength is one of the most fundamental methods to gain information on the chemical composition of a sample. The idea behind bulk absorption experiments is straightforward: the difference between incident and transmitted light gives the absorbance. However, when the concentration of absorbers is highly reduced, the sensitivity of the absorption experiment is limited by shot noise since the absorption cross-section of the absorbing molecules is small compared to the diffraction-limited area of the probing beam. Reaching the limit of a single absorber is often considered hardly possible. The main conceptual problem lies in the fact that the excitation wavelength and detection wavelength are exactly the same. This means that the relatively strong excitation light can't be cut with spectral filters and thus reaches the sensitive detector.

Contrary to the first single-atom and single-molecule absorption experiments, which used sophisticated triple [90] and double modulation [1, 25] techniques, followed only 10 years later by simpler single-modulation schemes [26, 27], the current experiment exploits the fact that the molecule emits part of the absorbed light at exactly the same wavelength as the excitation light, which leads to interference of the emitted light with the excitation light. Interferometric detection of single-molecule absorption [28, 91, 92] relies on the fact that the coherent part of the light emitted by the molecule can interfere in the far-field with the excitation light. By scanning the laser frequency over the molecular absorption, the phase difference between the two beams changes. The resulting absorption signal thus has a dispersive shape, which means that, depending on the phase difference, an absorption feature may be characterised by a decrease as well as an increase in signal.

In the mean time, single molecule detection by absorption at low temperatures using scanning near-field optical microscopy was proposed [93]. The main advantage of a near-field experiment would be the highly reduced size of the excitation spot, which can eventually go down to the same order of magnitude as the absorption cross-section of a single molecule. However, only the absorption of single, large self-assembled quantum-dots using scanning near-field optical microscopy at temperatures between 5 and 10 K has been reported so far [94, 95].

An alternative way to still detect the light emitted at the wavelength corresponding exactly to the purely electronic zero-phonon line is by excitation into a vibrational level of the first singlet excited state [96,97]. This involves weak absorption and broad single-molecule absorption lines, but allows to spectrally separate the signal and the excitation light.

In this chapter, a new sample aimed for single-molecule absorption spectroscopy is characterised, followed by an experiment in which single molecules are detected directly in absorption using an interferometric approach [28, 91, 92]. The absorption and Stokes-shifted fluorescence of single molecules are detected simultaneously. Single-molecule absorption and fluorescence excitation spectra show typical dynamics probably caused by spectral diffusion in the polymer host. A clear anti-correlation between the amplitude of the absorption signal and the width of single-molecule fluorescence excitation lines is observed. Some molecules appear to be visible in absorption only. The results demonstrate the feasibility of direct single-emitter absorption experiments and provide a clear picture of the underlying physics.

5.2 Requirements for single-molecule detection by absorption

The requirements for single-molecule detection by absorption at low temperature are largely similar to those for fluorescence. Crucial for the application of the interferometric technique is the coherent scattering of at least part of the absorbed light at exactly the same wavelength as the excitation. Implicitly, this requirement also holds for fluorescence experiments, as coherently scattered light interfering with the incoming excitation beam in the near-field of the molecule is responsible for the large absorption cross-section of a single molecule at low temperature.

An additional requirement for single molecule detection by absorption using an interferometric approach is a maximised absorption cross-section. A maximised absorption cross-section means that the largest ratio of absorption cross-section to excitation spot size is obtained. For a given molecule, the only controllable parameter that contributes to the absorption cross-section is the angle between the transition dipole moment and the incident electric field. As a result the orientation of single molecules in the matrix now becomes of vital importance. Ideally, the

transition dipole moment of a single molecule would be oriented parallel to the sample plane for absorption experiments using confocal microscopy. However, most of the impurity molecules in the systems studied so far turn out to be oriented unfavourably (terrylene in *p*-terphenyl [81,82]), to have unfavourable photo-physical properties (pentacene in *p*-terphenyl [39]) or to be delicate to prepare and to handle (terrylene in naphthalene [98]).

Mechanical treatment of polymeric materials, such as tensile deformation or rubbing, can be used to induce a high degree of uniaxial orientation of the polymer matrix, and likewise of form-anisotropic fluorescent guest molecules incorporated in the latter [99–101]. Recent room-temperature experiments on uniaxially oriented films of ultra-high molecular weight polyethylene (UHMWPE) doped with a poly(2,5-dialkoxy-*p*-phenylene ethynylene) derivative (EHO-OPPE) [102] have shown that even at the single-molecule level, the (in this case polymeric) fluorescent guest molecules tend to adopt the preferential orientation of the surrounding matrix after uniaxial tensile deformation of the sample.

5.3 Terrylene in a stretched film of linear low-density polyethylene

Terrylene in polyethylene is a well-known guest-host system that exhibits relatively narrow zero-phonon lines at cryogenic temperatures [84–86, 103, 104]. Rather interestingly, all previous studies concerning this system were performed on disordered materials. As was shown earlier, conventional melt-processing and subsequent tensile deformation of the resulting molecularly mixed blends of linear low-density polyethylene (LLDPE) and form-anisotropic fluorescent guest molecules allows production of thin films in which the guest molecules adopt a very high degree of uniaxial orientation [101]. Exploiting this general protocol, a new single-molecule system aimed for use at low temperature was produced. The orientational distribution as well as the stability, the line width and the saturation properties of terrylene molecules are measured at 1.8 K and, if applicable, at ambient conditions to characterise the new samples.

5.3.1 Absorbance spectrum

For practical purposes an absorbance spectrum of an unstretched film of LLDPE comprising 40 μg/g of terrylene was recorded at room temperature using a HP # 8453 spectrometer (see Fig. 5.1). Unfortunately the absorbance of the stretched films was too low to be detected by the apparatus and small changes in the spectrum due to the ordering that is induced by stretching can't be excluded. The main features in the spectrum are the two absorption peaks at 520 nm and 566 nm. The dye-laser (with Rhodamine 6G) only provides stable emission of light from 569 nm to about 605 nm. This means that in all experiments, excitation is in the wing of the absorption band at about 570 nm. As the widths of the bands relate to the amount of disorder in the sample [23], the molecules with the most common properties are expected to be located closest to the centre of the band. For this reason a film with a lower concentration was used in the low temperature experiment, such that single molecules could be monitored upon excitation at 570 nm.

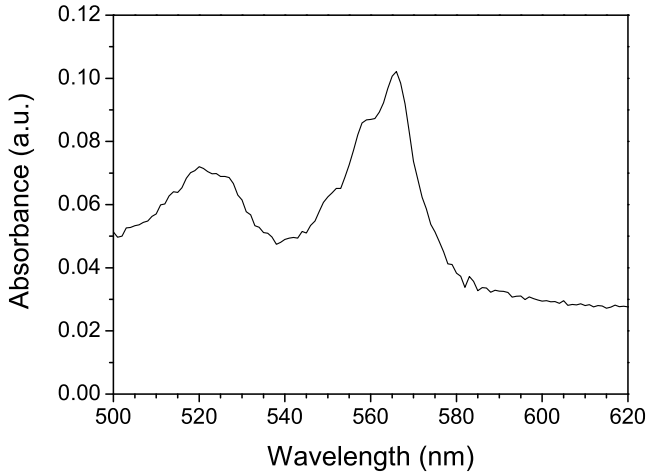

Figure 5.1: *Absorbance spectrum of an unstretched film of 40 μg/g terrylene in LLDPE at room temperature.*

5.3.2 Fluorescence excitation polarisation microscopy

A typical 340×340 μm^2 fluorescence excitation image of an LLDPE film comprising 1 μg/g of terrylene recorded at ambient temperature is displayed in Fig. 5.2A. Highly fluorescent, stripe-like structures with intermittent darker areas oriented parallel to the direction of tensile deformation (hereafter referred to as the orientation

direction of the film) are observed [102]. For this experiment, the orientation direction of the film was chosen to coincide with the direction of the electromagnetic field vector of the linearly polarised excitation light, which is used as a reference direction (relative polarisation 0°) in the following. The inset shows the emission for excitation with light polarised perpendicularly to the film's stretching direction. The pronounced contrast of these images reflects the high degree of orientation of an ensemble of terrylene molecules in the stretched LLDPE film. Similar images with the same depth of modulation were obtained on different parts of the film, indicating macroscopic homogeneity of the sample. Although these measurements only allow a definite assignment of the orientation of the absorption dipole projected onto the sample plane, it is expected that possible out-of-plane components are small.

The single-molecule detection level was not reached due to the broad absorption lines at ambient temperature, however the same sample was used for further studies at cryogenic temperatures, where single molecules with narrow zero-phonon lines were addressed by fluorescence excitation spectroscopy.

Fig. 5.2B shows a typical 34×34 μm^2 fluorescence excitation image of the same sample with the same polarisation directions at 1.8 K. It exhibits well-separated diffraction-limited fluorescence spots of variable intensity upon excitation with light polarised parallel (0°) to the orientation direction of the film, but no spots could be observed upon excitation with perpendicularly polarised light. To investigate this preferential orientation in more detail, a series of images was acquired by changing the polarisation direction of the excitation light in 18 steps of 10°. Only molecules that could be observed in the entire series of images were selected for further analysis. The orientation of the transition dipole moment of these molecules is determined by fitting the spots observed in the images to two-dimensional Gaussian functions using Igor Pro (Wavemetrics). The amplitude of the resulting two-dimensional Gaussians was then plotted as a function of relative polarisation. An example is shown in Fig. 5.2C. The data were fitted with a $\cos^2$ function, which allows for determination of the extremes. A minimum around 90° and a maximum around 0° can be observed. The result of each fitting procedure can be used to constructed a probability density function (pdf) [88] that specifies the probability of measuring a certain orientation of the transition dipole moment of a molecule. The normalized sum of all the pdfs obtained for different molecules results in an overall pdf that characterises the probability of finding a molecule with a certain orientation in the sample (see

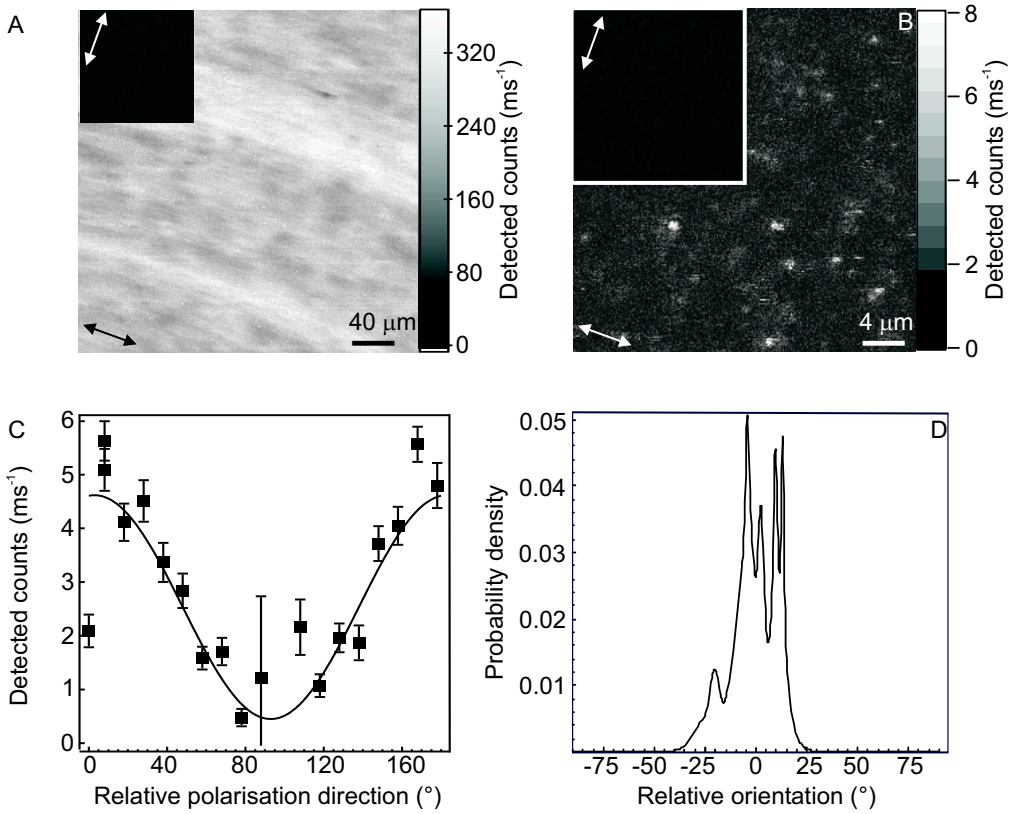

Figure 5.2: *(A) Scanning confocal optical microscopy image of a stretched (λ=10) film of LLDPE comprising 1 µg/g of terrylene at room temperature. The arrows denote the polarisation direction. (B) Scanning confocal optical microscopy image of the same film at 1.8 K. The integration time in (A) and (B) was 2.6 ms per pixel. The insets in A and B: excitation with the polarisation turned over 90°. (C) Modulation of the fluorescence of a single terrylene molecule as a function of the polarisation.(D) Probability density function of finding a single terrylene molecule with a certain orientation. The pdf is based on 22 molecules.*

Fig. 5.2D). The overall pdf exhibits a clear maximum around 0°, and indicates that the probability of finding molecules with a transition dipole moment outside the interval [-40°, 25°] is virtually zero. The narrow peaks displayed by the overall pdf are due to the fact that even the transition dipole moments of well oriented molecules show a slight deviation from the orientation direction of the sample. For example, the data shown in Fig. 5.2C translate into an offset of 3° ± 1° with respect to the film's axis.

5.3.3 Spectral stability

An important property of a single molecule system, in particular in view of quantum optics experiments, is the stability of the absorption frequency of single molecules over time. In polymers and glasses the stability of the absorption frequency is deteriorated by local degrees of freedom, which at cryogenic temperature can be modelled by two-level tunnelling systems that interact with the molecule via electric or strain fields [4]. To investigate the spectral stability, repeated 10 GHz scans were performed for about 75 minutes while recording the fluorescence. The result of this experiment is shown in Fig. 5.3.

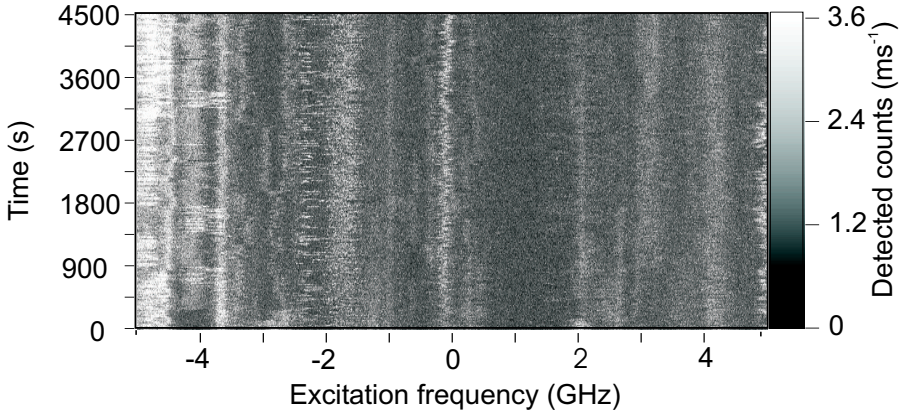

Figure 5.3: *Repeated fluorescence excitation frequency scan to monitor the stability of single molecules over more than 1 hour. Most molecules show a high degree of photo-stability. Some small jitter in the absorption frequencies of individual molecules can be observed. Only a few molecules undergo spectral jumps (e.g., the molecule at -3.4 GHz jumps to -3.0 GHz and back). The integration time was 8.5 ms per pixel.*

The excitation intensity is adjusted to be far below saturation in order to minimise photo-induced frequency jumps of the molecules. Fig. 5.3 reveals a number of interesting features displayed by terrylene molecules in an oriented LLDPE matrix. First of all, most of the molecules can be followed during the entire experiment, which means that no major frequency jumps take place. Second, the molecules are relatively stable in their absorption frequencies, staying all the time relatively close to the original value. Third, the molecules can be divided into two groups, according to the ranges in which the absorption frequencies vary. The absorption frequency of one group of molecules varies in a range of 130–160 MHz, while the other group of molecules shows variations of 300–450 MHz. Similar fluctuations over a spectral range of 50–400 MHz were reported in the literature [84]. However, it is not clear whether different ranges of fluctuations were observed for different molecules in this prior work. Finally, only few molecules undergo larger discontinuous frequency jumps, irrespective of their line widths. Examples are the molecule at −3.4 GHz that jumps to −3.0 GHz and back or the molecule at −4.8 GHz that jumps several times to −4.0 GHz and back. However, larger jumps over several GHz, as reported in reference [84] are not observed in these stretched samples. In conclusion, the stability of the molecule's absorption frequency doesn't reach that of crystalline matrices of low-molecular weight compounds (see e.g. [31]), however single molecules can be excited and followed over extended periods of time without problems.

5.3.4 Saturation behaviour

Saturation properties are relevant to achieve optimised experimental conditions and, more importantly for full sample characterisation, they can provide some insight into the out-of-plane component of the orientation of the molecular transition dipole moment [38]. Saturation data of single terrylene molecules were extracted from repeated frequency scans while varying the intensity. Typically, 5 to 10 frequency scans were recorded at each excitation intensity. From these spectra the emission rates and the line widths (Full Width at Half Maximum) of single molecules were determined by fitting to a Lorentzian line shape. Due to fluctuations in the absorption frequency of the molecules, there are variations in the line width and emission rate for one and the same molecule in separate frequency scans. For this reason, the values determined from at least 5 spectra at the same excitation intensity were averaged and the standard deviations were taken as a measure for the uncertainties

in these values. An example of saturation data is shown in the inset of Fig. 5.4. The fit was weighted by the uncertainties on the individual data points and yields the saturation intensity and the maximum emission rate with the respective uncertainties.

From the individual values of the saturation intensity and the homogeneous line widths with respective uncertainties, overall pdfs were constructed, as shown in Fig. 5.4A and B. The most probable saturation intensity is found at I = 70 mW/cm^2 and the most probable homogeneous line width is 126.3 MHz. The shoulder in the line width distribution around 200 MHz is consistent with the above discussion of Fig. 5.3. The probability density for line widths below the lifetime limit (about 50 MHz) is not zero due to the uncertainties on the homogeneous line widths. The latter are caused by the spectral jumping of the molecules during the time of a scan.

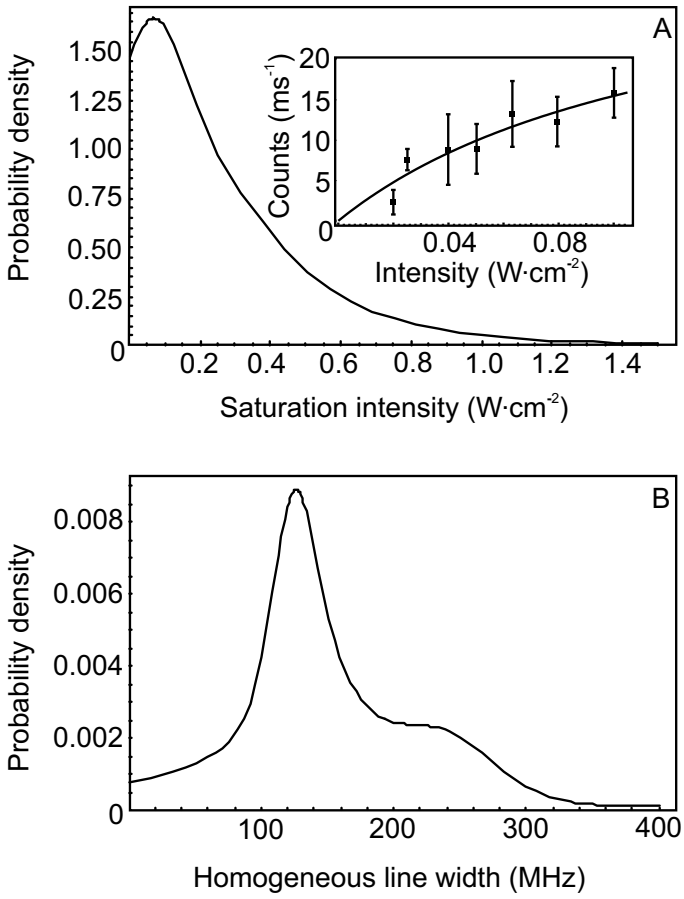

Figure 5.4: *(A) Probability density of finding a molecule with a given saturation intensity. The inset shows a typical saturation curve of the detected emission rate vs excitation intensity. Data points are obtained from the average of the detected emission rates of at least 5 frequency scans. (B) Probability density of finding a molecule with a given line width. The most probable homogeneous line width is clearly broader than the life-time limited line width. A shoulder at 200 MHz suggests the existence of a second population of molecules sitting in less favourable environments.*

The range of observed homogeneous line widths in the stretched LLDPE samples is comparable to the values reported in the literature for disordered guest-host

systems of terrylene in different polyethylenes [84, 85]. The most probable homogeneous line width that was obtained for terrylene molecules in a stretched film of 1 μg/g terrylene in LLDPE is close to the average homogeneous line width reported for terrylene incorporated in a disordered high-density polyethylene matrix [85] and slightly broader than the most frequently observed homogeneous line width found for the latter system. On the other hand, the most probable homogeneous line width determined here is at the lower limit and partly below the range quoted for terrylene dispersed in a low-density polyethylene [84]. This suggests that the terrylene molecules in stretched films of LLDPE are experiencing a local environment which is more ordered than in low-density polyethylene [84]. In fact, the local order is comparable to that found in higher density, i.e. more crystalline, polyethylene [85], but with the important additional feature of having the transition dipole moments of the terrylene molecules all lined up.

5.3.5 Conclusion on the sample structure

The high degree of optical anisotropy displayed by the oriented terrylene-doped LLDPE samples and the fact that the absorption maxima of terrylene ensembles and single terrylene molecules coincide with the orientation direction of the sample clearly indicate that the terrylene molecules are oriented with their geometric long axis parallel to the sample axis and that the optical transition dipole moment of terrylene matches with the geometric long axis of the molecule, in agreement with Ref. [105]. The data further suggest that the off-axis components of the transition dipole moment of terrylene are very small. The films display so-called "fibre symmetry". While all the terrylene molecules are oriented with their long axes parallel to the orientation direction, they can freely rotate around this axis. So the "planes" of the terrylene molecules are not parallel to the film plane, but rotate around the long axis. However, the projected dipole moment of a single terrylene molecule is identical if looked at from the "face" and from the "edge". This finding is further supported by the analysis of the saturation intensity (see section 5.3.4) which is not only important from an experimental point of view, but also provides some insight into the three-dimensional orientation of the fluorescent molecules with respect to the laboratory coordinates [38]. Indeed, the intrinsic saturation intensity of terrylene, i.e. of a single terrylene molecule oriented parallel to a substrate, was estimated to be 80 $\pm$ 30 mW/cm^2 [38]. Gratifyingly, the saturation intensity that was exper-

imentally determined in this sample, 70 mW/cm^2, is in good agreement with this value, consistent with the fact that the terrylene molecules in uniaxially deformed samples indeed feature negligible out-of-plane components of their transition dipole moments. This architecture results in an optimised absorption cross-section, as is desirable for the direct detection of single molecules by absorption.

5.4 Interferometric approach to single-molecule detection by absorption

The interferometric approach to single-molecule detection by absorption [28, 91, 92] relies on the fact that the coherent part of the light scattered by a single molecule interferes in the far field with part of the excitation light. Typically up to 4% of the excitation light is reflected by the surface of the sample, as is illustrated in Fig. 5.5.

This amount suffices to act as one arm of an interferometer, whereas the molecule acts as the other arm. At constant frequency, the phase difference between the coherently scattered light and the reflected light is constant. However, on scanning the laser frequency, the phase difference between the two beams changes. As a result, the presence of a molecule leads to an interference signal in which the phase difference is changing. A single molecule is thus seen as a dispersive signal. The amplitude of the interference signals depends on the relative amplitudes of the signal and reference beams.

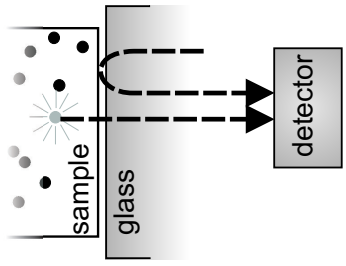

Figure 5.5: *A weak reflection from the sample surface acts as reference signal.*

Similar in its basic principles is the situation in which an additional external reference beam is used. The external reference beam is generated by retro-reflection of the light that is transmitted by the glass wedge and overlapped with the light scattered coherently by the molecule and the light reflected from the sample surface on the detector. The mirror that retro-reflects the light stands on a piezo-controlled translation stage and thus permits precise control of the path length. The main advantage of the external reference beam is the control of the phase difference (via

path length) between the light scattered by the molecule and the reference beam. This additional external reference beam was blocked in part of the experiments.

A full theoretical description of the expected signals is given in Ref. [28]. The emitter is treated as a classical dipole emitting light with a characteristic phase depending on the detuning. Interference with the reference beam leads to dispersion-like resonance peaks in the absorption signal, which are, after background subtraction, described by:

$$R(\omega) = -2A\Gamma_0 \cdot \frac{\Gamma_0 \sin\varphi + (\omega_0 - \omega)\cos\varphi}{\Gamma_0^2 + (\omega - \omega_0)^2} \tag{5.1}$$

where A denotes the amplitude of the absorption signal via $A = \sqrt{R_0 \cdot R_{ref}}$, Γ_0 the half width at half maximum, ω the laser detuning, ω_0 the resonance frequency and φ the phase difference between the molecular emission and the reference beam. Both ω_0 and Γ_0 are determined from simultaneously recorded fluorescence excitation spectra by fitting with a Lorentzian whenever possible. Depending on the phase difference an absorption feature may be characterised by a decrease as well as by an increase of the absorption signal.

5.5 Results

5.5.1 Spectroscopy

A typical example of simultaneously recorded fluorescence-excitation and absorption spectra without external reference is shown in Fig. 5.6A. All molecules found in the fluorescence excitation spectrum are fitted by a Lorentzian line-shape yielding the resonance frequency and line width. The corresponding absorption signals were fitted using Eq. 5.1 with phase difference, φ, and amplitude, A, as free parameters. Prior knowledge of the resonance frequency and the line width of a single molecule is helpful to identify true absorption features. The absorption spectrum in Fig. 5.6A shows some degree of shot noise (grey area), however, several peaks are clearly distinct from noise due to their larger amplitude and high correlation with the fluorescence excitation spectrum. Spectral instabilities, as expected for a polymeric host material [4], are clearly visible in the wings of the lines at 166 MHz

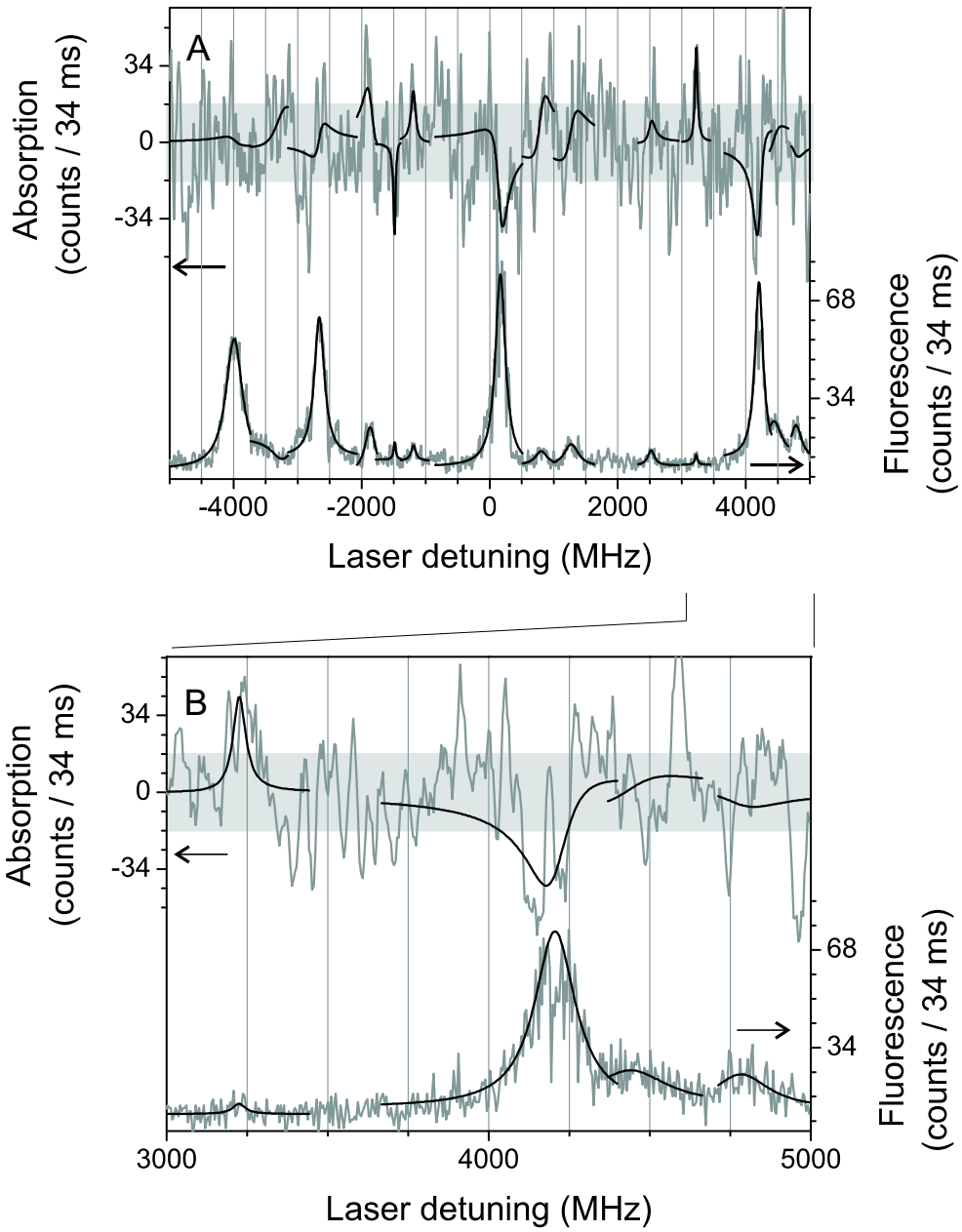

Figure 5.6: *(A) Simultaneously recorded fluorescence excitation (lower trace, right axis) and absorption spectra (upper trace, left axis). No external reference beam was used. The solid black lines are fits to the data. Prior to fitting the absorption signal a slow cosine modulation, probably due to some interference on optical elements, with a period far longer than the 10 GHz range of the frequency scan was subtracted. The light grey box indicates the $\pm\sigma$ limits of the shot-noise. The integration time was 34 ms per point. (B) Zoom on the signals of a molecule that is blinking during the laser frequency scan.*

and −2661 MHz. These instabilities are observed in both simultaneously recorded signals. In the wing of the bright molecule centred at 166 MHz, the fluorescence suddenly drops. At exactly the same frequency, a sudden change in the absorption signal (going to almost 0) is observed. The same holds for the wings of the molecule at −2661 MHz, where all signals in the wings of the fluorescence line can be correlated in position and width to events in the absorption spectrum. A zoom on the frequencies between 3000 and 5000 MHz reveals that the molecule at 4203 MHz shows a blinking event (see Fig. 5.6B). The fluorescence intensity decreases around the maximum of the Lorentzian and simultaneously the absorption signal also jumps to zero-level.

Some events in the absorption spectrum can't be correlated directly to signals in the fluorescence excitation spectrum, like the pronounced dips at −4780 MHz, −1750 MHz, −535 MHz and 2860 MHz. Such contributions are ascribed to single molecules of which the Stokes-shifted fluorescence is too weak to be observed, probably because the fluorescence is cut by the Notch filter. In conclusion, the absorption spectrum that looks noisy and rather "empty" on a first glance, actually seems to show rich molecular absorption signatures.

As spectral instabilities can be expected for a polymeric host material [4], an easy criterion to state whether a signature in the absorption spectrum MUST be a molecule or not based on the line-width can't be used. Molecules jumping in and out of resonance would, with this criterion, all be classified as noise, although the occurrence of spectral jumps is obvious from Fig. 5.6A and Fig. 5.3. For a similar experiment performed on a single crystal, noise and molecules would easily be separated on the basis of the line width only.

Since the amount of coherently scattered light decreases upon saturation or due to dephasing, a negative correlation between the line width (as determined from the fluorescence excitation spectrum) and the amplitude of the absorption signal would be expected. A scatter plot of the data points from all fitted molecules in the spectra in Fig. 5.6A is shown in Fig. 5.7. A clear negative correlation between line width and absorption amplitude is indeed found.

An example of simultaneously recorded absorption and fluorescence excitation spectra with external reference beam is shown in Fig. 5.8. The two spectral traces were recorded immediately after each other. Again, dynamic processes are clearly

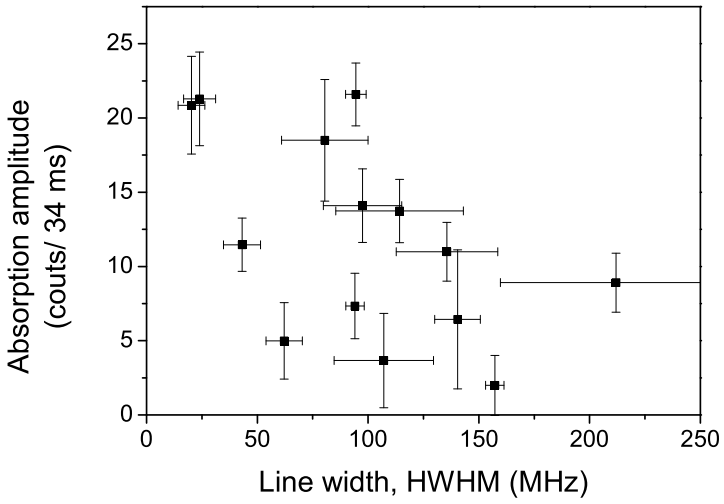

Figure 5.7: *Correlation between the amplitude of the absorption signal and the line width (HWHM) of the single-molecule resonance. The data points are taken from the spectrum in Fig. 5.6(A).*

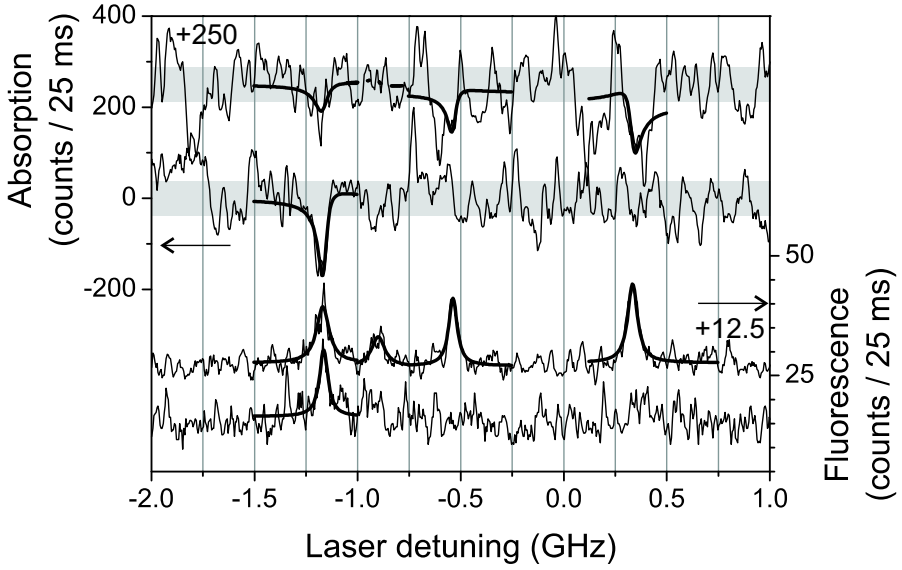

Figure 5.8: *Two consecutive sets of simultaneously recorded fluorescence (lower traces, right axis) and absorption spectra (upper traces, left axis) with external reference beam. The grey boxes indicate the $\pm\sigma$ limits of the shot-noise in the absorption signal. Offsets were added for better visibility. The thicker black lines are fits to the data. The integration time was 25 ms per point.*

observed. Due to the larger path difference between the arms of the interferometer, the absorption signal showed a cosine-modulated background with a short period. The spectra displayed in Fig. 5.8 are the results after background subtraction. In the first fluorescence excitation spectrum (lowest trace) one weak molecule was found. In the corresponding absorption spectrum, a dispersive absorption signature, which is clearly above the noise level, is observed only at the position of this molecule. In the spectrum that was taken immediately after, more molecules appear. The molecule that was also found in the previous scan now has a reduced amplitude and an increased line-width in fluorescence. The strong effect on the absorption signal is seen immediately: the amplitude is highly reduced in the second absorption spectrum (upmost trace). Two of the remaining molecules that are observed in fluorescence (at -0.54 GHz and at 0.33 GHz) are also observed in absorption. However, the remaining molecule in the fluorescence spectrum, at -0.90 GHz, which shows a rather broad signal, is not visible in absorption probably due to the large dephasing it is subjected to. Several features in the absorption spectrum (upmost trace) are attributed to single molecules that are not observed in fluorescence. Examples of such signals are the strong dips at about -1.80 GHz and 0.13 GHz and the dispersive feature at about -0.65 GHz.

5.5.2 Time trace

A time trace of fluorescence and simultaneously recorded absorption is shown in Fig. 5.9. The rather low fluorescence signal suggests that this particular molecule was excited in the wing of its resonance. The strong fluctuations in both fluorescence and absorption are attributed to spectral diffusion of the molecule since there is a strong correlation between the fluctuations in fluorescence and absorption. A slow decrease in the fluorescence signal due to piezo drift of the sample scanner is observed, followed by a jump to the background level at about 18690 ms. With the same slope, the absorption signal increases over the same period of time, until it jumps to a constant value. The constant high level is the background signal with the molecule most of the time absent. As the phase difference between molecule and reference was constant, no background subtraction was performed in the data analysis.

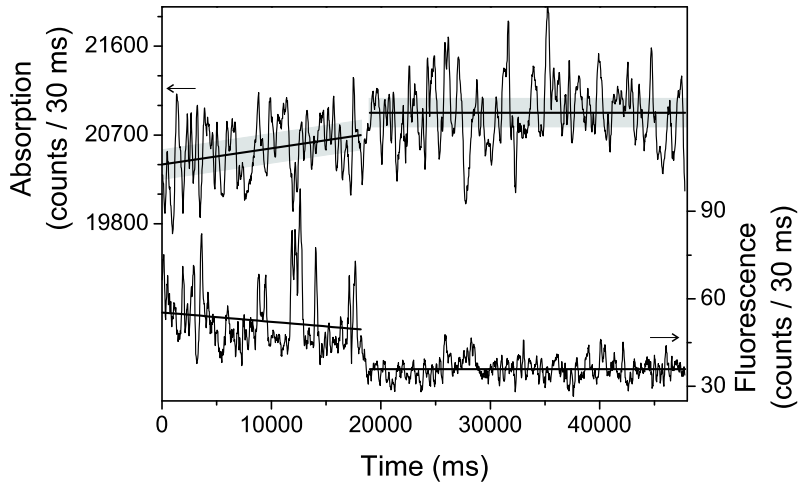

Figure 5.9: *Simultaneously recorded time trace of a single molecule in absorption (upper trace, left axis) and in fluorescence (lower trace, right axis). The beginning of the traces was fitted to a single exponential function with the same coefficients in both traces. The horizontal lines after the spectral jump are averages of the remaining trace. The grey boxes indicate the $\pm\sigma$ limits of the shot-noise in the absorption signal. The integration time was 30 ms per point.*

5.6 Conclusion

Simultaneous recording of absorption and fluorescence of single molecules at low temperature was demonstrated for the first time. Simultaneous recording provides the exact resonance frequency and line width of a single-molecule resonance if Stokes-shifted fluorescence can be detected. Using this information the phase difference between the coherently scattered light and the reference can be extracted. Furthermore, the measurement time was reduced by a factor of 20 as compared to the literature [92]. The fast measurement allows to observe dynamical processes that would be averaged out otherwise. The spectral instabilities of terrylene in polyethylene lead to a "noisy" appearance of the data that should not be misinterpreted as system noise. Additionally, single molecules could be detected in absorption that show no detectable Stokes-shifted fluorescence.

6. Aperture scanning near-field optical microscopy and spectroscopy of single molecules

Single-molecule microscopy and spectroscopy using an aperture scanning near-field optical microscope operating at 1.8 K in a helium bath cryostat is demonstrated. From near-field microscopy images at constant excitation frequency, the orientation of single molecules can be deduced. Spectral information is obtained using both near-field and confocal excitation schemes by scanning the excitation frequency at a fixed sample position. Differences between near-field and confocal spectra are explained in terms of the position with respect to the aperture and the molecular orientation.

6.1 Aperture scanning near-field optical microscopy

Aperture scanning near-field optical microscopy was proposed by Synge in 1928 [106] to overcome the classical diffraction limit as formulated by Abbe in 1873 [44]. A theoretical description of the fields behind a circular sub-wavelength aperture in an infinitly large and conducting screen was formulated by Bethe in 1944 [57] and corrected by Bouwkamp in 1950 [58]. The first experimental realization was achieved in 1984 by Pohl and co-workers [11] and independently by Lewis and co-workers [51]. Aperture scanning near-field optical microscopy of single molecules has proven to be a powerful technique, as it can show not only the position, but also the three-dimensional orientation of the transition dipole moments of single molecules [10, 107] while the resolution is determined by the size of the aperture [56]. This capability of high resolution imaging due to the fact that the size of the excitation spot is of the size of the aperture has an intriguing consequence: the size of the excitation spot gets of the same order of magnitude as the absorption cross-section of a single molecule at cryogenic temperatures. Thus, scanning near-field optical microscopy and spectroscopy was proposed to detect single molecules at low temperature in absorption [93]. However, single-molecule near-field optical microscopy and spectroscopy at temperatures below 2 K is not yet a well established technique and first a proof of the capability to do fluorescence studies with the instrument is required.

So far, much work has been performed at room temperature (for reviews see [108, 109]) and at temperatures down to 5 K. For the latter case, research focussed mainly on quantum wires [110–112] and quantum dots [113,114]. For single-molecule spectroscopy, the interesting temperature range is even lower than 5 K, as the line width of the zero phonon lines gets close to the lifetime-limited value only at temperatures below 2 K [4]. The general interest in high-resolution spectroscopy at temperatures below 2 K is demonstrated by the number of descriptions of scanning near-field optical microscopy set ups, aimed for operation in this temperature range [71,72,115,116]. Unfortunately the number of reported scanning near-field optical microscopy experiments at temperatures of 2 K or lower is very small. So far at these temperatures, quantum wire- [117] and single-molecule near-field optical spectroscopy were demonstrated [16]. However, in the latter study, no direct comparison

of near-field and confocal spectra was shown to demonstrate directly the increase in resolution and no single-molecule near-field imaging was possible with the set up. In this chapter, scanning near-field optical microscopy of single molecules and a direct comparison between near-field and confocal single-molecule fluorescence excitation spectra at 1.8 K in a helium bath cryostat are discussed. The system under study is a crystalline sample of terrylene in *p*-terphenyl. The preparation of these crystals is described in section 3.5.1. The main properties of this system will be described together with the aperture scanning near-field optical microscopy measurements in section 6.3.1.

6.2 Tip and tip alignment

The tip used in this experiment was prepared as described in section 3.3.1. It had an elliptical aperture with dimensions of about 300 nm in the long and about 100 nm in the short direction (see Fig. 6.1A). For rectangular slit-like apertures, the transmitted light was found to be mainly polarised along the short direction of the aperture [60], in agreement with theoretical predictions [59]. From this finding, the light coming through the tip is supposed to be strongly elliptically polarised with a main component along the short axis of the aperture. The field distribution at the aperture shows strong field components along the fibre axis perpendicular to the sample surface at the rims on the sides of the aperture and field components parallel to the sample in the centre of the aperture [10, 57, 58]. As a direct consequence, molecules with transition dipole moments perpendicular to the sample surface are expected to be imaged as two lobes situated beneath the rims of the aperture [10]. The distance between the lobes thus reflects the diameter of the aperture and the tip-molecule separation.

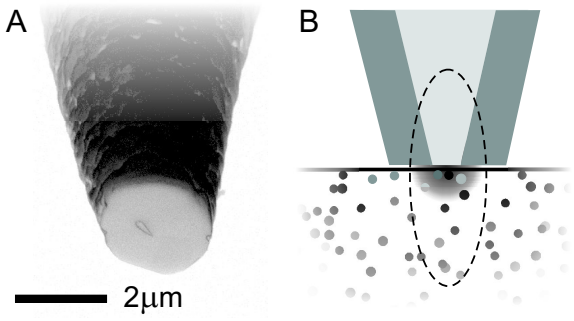

Figure 6.1: *(A) SEM image of the tip that was used for the experiment. (B) The illuminated areas in confocal (dashed line) and near-field excitation. After careful alignment, the volume that is excited in the near-field is a fraction of the volume excited in the confocal configuration.*

A critical part for the comparison of confocal and near-field images/spectra is the overlap of the volumes under study (see Fig. 6.1B). During confocal measurements, light was focussed on the upper side of the *p*-terphenyl crystal, which is the surface that is also accessible to the near-field probe. First, by confocal scanning, an area on the crystal was searched in which a number of molecules could be seen in excitation-frequency scans as well as in sample scan images at constant frequency. After that, the objective was moved 3 μm up such that the focus was positioned above the sample by the same amount. The excitation light was then sent into the fibre for near-field excitation and with the help of the light coming through the aperture, the tip was positioned above the confocal excitation spot using the CCD camera. Finally, the tip was moved towards the sample using a slip-stick drive until the tip appeared to be in focus by minimizing the emission spot on the CCD ($\approx$3 μm above the sample surface). At this point, the objective was moved back such that upper surface of the crystal was in focus again. For the remaining part of the tip approach, fluorescence excitation spectra were taken in order to make use of the change in the fluorescence background [16] as a measure for the tip-sample distance. At small gap-widths, when single-molecule peaks already appeared in the spectra, a tuning fork detected shear-force signal was monitored and the gap width was adjusted to a value just before shear-force contact occurred.

6.3 Results

6.3.1 Aperture scanning near-field optical microscopy of single molecules

An example of a 20 μm sample scan under near-field excitation at constant frequency is shown in Fig. 6.2. Signals from single molecules appear either as a single spot or as a closely spaced two-lobe pattern, often with unequal intensities in the lobes. Similar patterns have been observed in single molecule scanning near-field optical microscopy at room temperature [10, 107] and were attributed to the orientation of the transition dipole moments of single molecules. As the terrylene molecules in the O_2 site of a *p*-terphenyl crystal are expected to be oriented almost perpendicular to the substrate [81, 82], mainly two-lobe patterns with nearly equal intensities in the lobes are expected. This is indeed the pattern found for most molecules in the image.

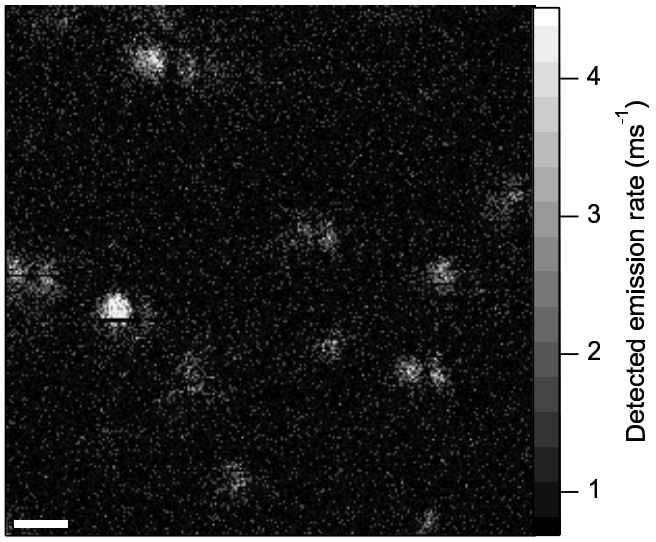

Figure 6.2: *Scanning near-field optical microscopy image of single terrylene molecules at 1.8 K. The symmetric two lobe patterns of most spots point towards a transition dipole moment orientation perpendicular to the sample plane. However, some molecules show different patterns, indicating deviating orientations. The scale bar is 2 μm, the integration time was 2.6 ms/pixel.*

However, single spots, indicating a parallel orientation, and two-lobe patterns with clearly unequal intensities, indicating an intermediate orientation, are also found. The finding of the distinct patterns is already a proof for the fact that a well-defined absorption dipole moment is involved. A second check is that on changing the excitation frequency in steps of 20 MHz, the patterns change in intensity, as the molecules go in or out of resonance, but the relative intensities in the lobes of each pattern remain constant. This clearly indicates that single molecules with narrow zero-phonon lines are observed. The patterns that indicate an orientation of single molecules other than (almost) perpendicular to the substrate are attributed to molecules sitting at imperfections in the crystal.

6.3.2 Aperture scanning near-field optical spectroscopy of single molecules

Near-field optical spectroscopy was used during tip approach to estimate the tip–sample distance. All spectra presented in this section were taken directly after the tip approach and before any spatial scanning of the tip was performed. Thus, tip damage before or during frequency scans can be excluded. Fig. 6.3 shows two examples of typical 20 GHz fluorescence excitation spectra in both confocal and near-field excitation. Zero detuning was at about 578.5 nm and all spectra were repeated at least once to check the reproducibility of the spectral positions and relative intensities of the single molecules. The excitation intensity in confocal spectra was above saturation, whereas in the near-field excitation spectra, extreme care was taken to

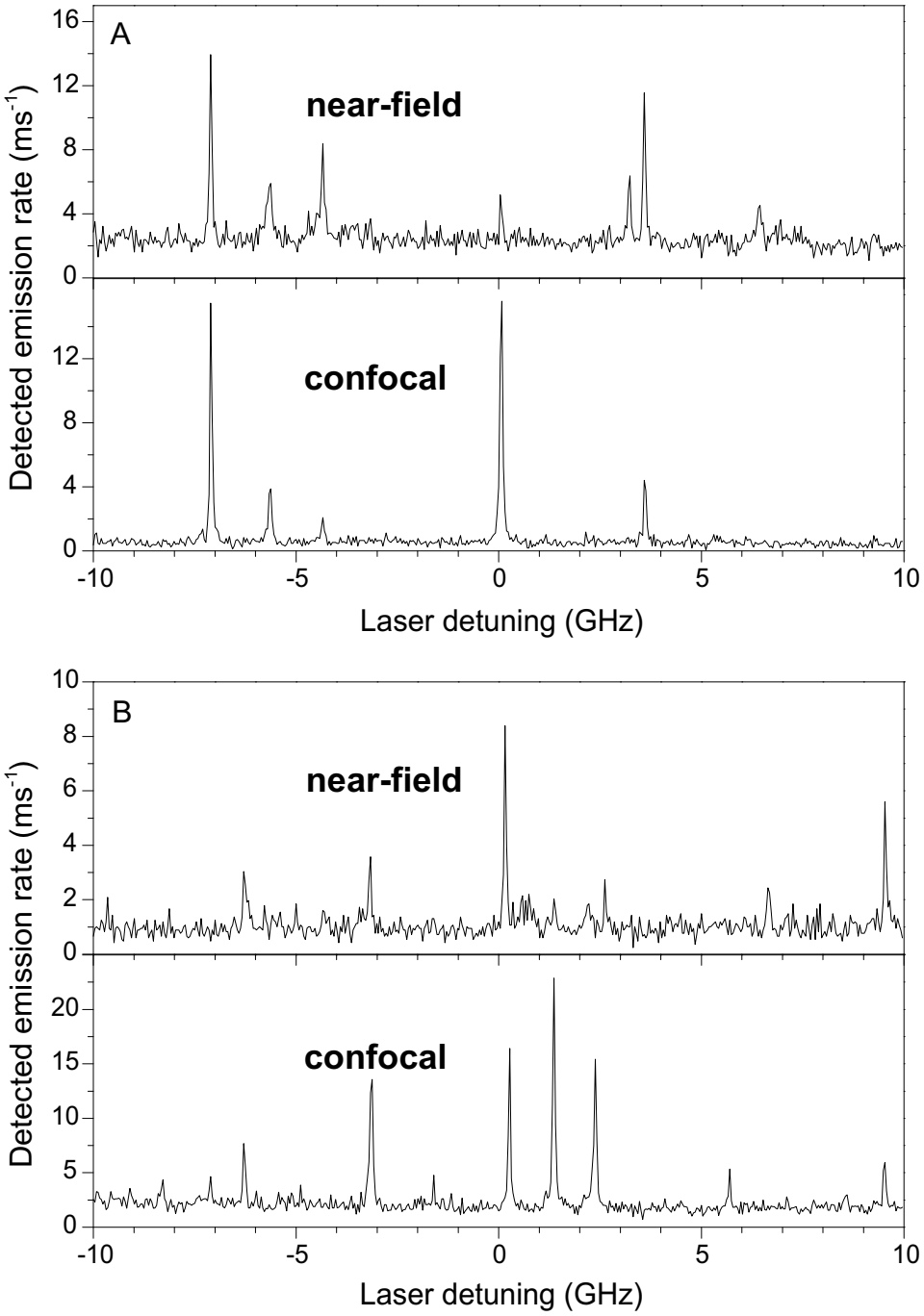

Figure 6.3: *(A) and (B) Examples of near-field and confocal fluorescence excitation spectra. The excitation frequency was scanned over 20 GHz and the integration time was 16.9 ms. The intensity in the confocal spectra was above saturation. Between the spectra in (A) and (B), only the laser frequency was changed.*

keep the intensity below the saturation level, to prevent intensity induced spectral instabilities. In Fig. 6.3A, more single-molecule lines are found upon near-field excitation (upper trace) as compared to confocal excitation (lower trace). Besides, the relative intensities of the molecules that appear in both excitation schemes are different. Although a higher number of molecules in a near-field excitation scan might appear counter-intuitive, it can be explained well by the nature of the excitation and the characteristics of the sample. Since a major part of the field components of light emanating from a sub-wavelength aperture is oriented perpendicular to the sample surface and are concentrated at the aperture rims [10], molecules with their transition dipole moments oriented almost perpendicular to the sample plane, such as terrylene molecules in the O_2 site of the *p*-terphenyl crystal [81,82] can be excited efficiently if they are located close to the rim of the aperture. On the other hand such molecules are excited very inefficiently in a confocal scheme with predominant transverse polarisation. However, the differences in intensity cannot be explained by this reason alone. Another important influence is the difference in excitation volume (Fig. 6.1B). Molecules that appear weaker in the near-field spectra can either have a relatively unfavourable orientation, depending on the relative position between aperture and molecule, or can be located further away from the tip, or a combination of both. Unfortunately, the relative position and relative orientation cannot be separated using fluorescence excitation spectroscopy only.

Fig. 6.3B shows another example of near-field and confocal fluorescence excitation spectra at the same spatial position, however, at a slightly different frequency. In this example fewer molecules are observed on near-field excitation. Three weak signatures can be found that are not seen under confocal excitation, whereas two intense lines in the confocal scans are almost absent in the near-field scans. The two intense lines seen in the confocal spectrum but absent in the near-field spectrum can most probably be attributed to two molecules positioned far from the sample surface, such that they can be excited with confocal excitation, but not with near-field excitation (see Fig. 6.1B). For the weaker signatures at a detuning between 6.5 and 8 GHz, the situation is different. They were found in the near-field spectrum, but not in the confocal spectrum. As the near-field excitation volume is a small part of the confocal excitation volume (see Fig. 6.1B), the positions of these molecules can't be the reason. Molecules that are inaccessible to confocal excitation although they reside within the confocal volume must have transition dipole moments almost perpendicular to the sample surface. In order to be visible in the near-field spectrum,

these molecules must be located close to the aperture rims. Note that in between the recording of the spectra of Fig. 6.3A and B, only the laser frequency was changed, while the tip and sample were both kept at the same position, indicating the absence of any conceivable artefacts.

6.4 Conclusion

In this chapter the first scanning near-field optical microscopy images of single molecules at 1.8 K have been shown. Such images give information on the position and orientation of the molecules in the scanned area, as was expected from room temperature scanning near-field optical microscopy images [10, 107]. Although the resolution is not much improved compared to far-field techniques due to the big aperture size, near-field effects are present as is reflected by the patterns from which the three dimensional orientation of single molecules could be deduced. Besides, a direct comparison between confocal and near-field fluorescence excitation spectra has been shown for the first time. Differences between the molecules that were found in these spectra could be explained by a combination of orientation and position with respect to the aperture probe.

7. Outlook

The work presented in this thesis opens several possibilities for further single-molecule experiments at cryogenic temperatures, using both near-field and confocal techniques.

In a confocal experiment, it would be interesting to directly image single molecules in absorption. An idea would be to deduce the presence of a single molecule from a comparison between two images, of which it is known that in one image, the molecule was present, while in the other it was not. However, Rayleigh scattering played a too prominent role in the samples studied in this thesis, resulting in structures in the backscattered light. Unfortunately, on changing the wavelength by a few tens of MHz, the backscattered image was changed enormously, making it impossible to use the wavelength as a parameter to control the molecules which are in resonance in the image. Another option, to make molecules undergo spectral jumping (by high intensity illumination between two images), proved to reduce the changes in the scattering images, however, the results were not yet convincingly beyond the noise level.

A more favourable solution, would be to look at molecules in a thin uniform film that is adhering to the glass cover-slip over its full length uniformly, such as a spin-coated sample. On one hand, the problem of having all molecules oriented in the same direction and possibly close to parallel to the substrate now comes back into play, however, the number of surfaces from which light is reflected back is reduced (the upper-side of the glass cover-slip coinciding with the lower surface of the sample) and the flatness of the sample-surfaces would be highly increased, resulting in a more uniform reflection. Using such a sample, imaging of single molecules in absorption could become feasible, with similar or better signal-to-noise ratios (depending on the spectral stability of the molecules) than in the single-molecule absorption-spectroscopy presented in chapter 5.

An obvious experiment after the work on absorption (see chapter 5) and on scanning near-field optical microscopy and spectroscopy (see chapter 6) would be the combination of the two, or, in other words, to use near-field excitation for single-molecule detection by absorption [93]. As only molecules in close proximity to the sample surface can be addressed by near-field techniques, a thinner sample would be required. However, the requirement for the orientation is relaxed for near-field experiments, as the direction of the electric field anyway depends on the position with respect to the tip. Using a small aperture, the excitation light source could get

smaller than the absorption cross-section of a single molecule. It is expected that this would result in a highly improved signal-to-noise ratio.

In another experiment, which could be performed either on a confocal set up or on a near-field set up, changes in the choice of the guest-molecules seem to be feasible. This could be into the direction of molecules that emit a larger part of the fluorescence as resonance fluorescence and less Stokes-shifted fluorescence. It would be expected that a larger amount of light is available for interferometric detection, leading to a better signal-to-background ratio. In this way, the number of single-molecule systems suitable for low-temperature studies could be increased. A problem might be that the usual quick checks on the stability and determination of the line-width, which so far were done using a cut-off filter to detect only Stokes-shifted fluorescence, get more difficult.

As the field of single molecule detection at low temperature using a scanning near-field optical microscope is actually brand new, several fundamental questions remain to be answered. For these experiments, an especially interesting situation would be in the direct comparison with confocal data on the same molecule taken under the same conditions to learn about the influence of the rather large metal surface of a near-field tip in close proximity to the molecules under study. Experiments could focus on whether the homogeneous line-width of the molecules is changed under near-field excitation compared to the confocal case (with the tip retracted!). This would reveal eventual changes in the life-time due to other radiative or non-radiative decay paths that are being opened by the close proximity of the metal cladding of the tip. Such influences due to the presence of the tip have been observed at room temperature and lead to both shortening and lengthening of the fluorescence lifetimes [118–120]. A similar experiment could be to track changes in the relative intensities in the emission spectra of single molecules due to the presence of the tip (change in Franck-Condon factor). Another obvious question would be, whether the spectral stability of single molecules is affected by the presence of the tip and the influence of the tip-sample distance on all the above mentioned questions. A last parameter that might be difficult to track, could be the thickness of the metal coating. To see this effect, good statistics would be needed on all experiments.

Alternatively, the SNOM could simply be used as a tool for high resolution microscopy, in which the three-dimensional orientation and the spatial position of molecules is determined. This could be of interest for the study of host-guest sys-

tems, in which the structure or amount of order of the guest molecules is the property of interest. That is, when the molecules are used as a sensitive local probe that reflects the structure of its environment. The advantage of using SNOM for such experiments over the confocal microscope would of course be, that SNOM directly maps the orientation in all three dimensions, whereas in confocal microscopy, the projection of the transition dipole moment on the sample plane is measured. The third dimension can be deduced from saturation measurements, however, it requires a lot of work to collect saturation data for every single molecule under study in a sample.

Bibliography

[1] W. E. Moerner and L. Kador, "Optical Detection and Spectroscopy of Single Molecules in a Solid," *Phys. Rev. Lett.*, **1989**, *62* (21); 2535–2538.

[2] M. Orrit and J. Bernard, "Single Pentacene Molecules Detected by Fluorescence Excitation in a *p*-Terphenyl Crystal," *Phys. Rev. Lett.*, **1990**, *65*; 2716–2719.

[3] W. E. Moerner and T. Basché, "Optical Spectroscopy of Single Impurity Molecules in Solids," *Angew. Chem. Int. Ed. Engl.*, **1993**, *32* (4); 457–476.

[4] T. Basché, W. E. Moerner, M. Orrit and U. P. Wild, eds., *Single–Molecule Optical Detection, Imaging and Spectroscopy*, VCH Verlagsgesellschaft, Weinheim, **1997**.

[5] J. L. Skinner and W. E. Moerner, "Structure and Dynamics in Solids As Probed by Optical Spectroscopy," *J. Phys. Chem.*, **1996**, *100*; 13251–13262.

[6] T. Plakhotnik, E. A. Donley and U. P. Wild, "Single-Molecule Spectroscopy," *Ann. Rev. Phys. Chem.*, **1997**, *48*; 181–212.

[7] W. E. Moerner and M. Orrit, "Illuminating Single Molecules in Condensed Matter," *Science*, **1999**, *283*; 1670–1676.

[8] P. Tamarat, A. Maali, B. Lounis and M. Orrit, "Ten Years of Single-Molecule Spectroscopy," *J. Phys. Chem. A*, **2000**, *104* (1); 1–16.

[9] C. Brunel, P. Tamarat, B. Lounis and M. Orrit, "Optical spectroscopy of single molecules: application to nonlinear and quantum optics," *J. Lumin.*, **2000**, *87–89*; 105–108.

[10] E. Betzig and R. J. Chichester, "Single Molecules Observed by Near-Field Scanning Optical Microscopy," *Science*, **1993**, *262* (5138); 1422–1425.

[11] D. W. Pohl, W. Denk and M. Lanz, "Optical stethoscopy: Image recording with resolution $\lambda/20$," *Appl. Phys. Lett.*, **1984**, *44*; 651–653.

[12] G. Binnig, H. Rohrer, C. Gerber and E. Weibel, "Surface Studies by Scanning Tunneling Microscopy," *Phys. Rev. Lett.*, **1982**, *49* (1); 57–61.

[13] G. Binnig, C. F. Quate and C. Gerber, "Atomic Force Microscope," *Phys. Rev. Lett.*, **1986**, *56* (9); 930–933.

[14] G. Binnig, C. Gerber, E. Stoll, T. R. Albrecht and C. F. Quate, "Atomic resolution with atomic force microscope," *Europhys. Lett.*, **1987**, *3* (12); 1281–1286.

[15] N. Hosaka and T. Saiki, "Near-field fluorescence imaging of single molecules with a resolution in the range of 10 nm," *J. Microsc.*, **2000**, *202* (2); 362–364.

[16] W. E. Moerner, T. Plakhotnik, T. Irngartinger, U. P. Wild, D. W. Pohl and B. Hecht, "Near-Field Optical Spectroscopy of Individual Molecules in Solids," *Phys. Rev. Lett.*, **1994**, *73* (20); 2764–2767.

[17] A. M. van Oijen, J. Köhler, J. Schmidt, M. Müller and G. J. Brakenhoff, "3-Dimensional super-resolution by spectrally selective imaging," *Chem. Phys. Lett.*, **1998**, *292*; 183–187.

[18] A. M. van Oijen, J. Köhler, J. Schmidt, M. Müller and G. J. Brakenhoff, "Far-field fluorescence microscopy beyond the diffraction limit," *J. Opt. Soc. Am. A*, **1999**, *16* (4); 909–915.

[19] A. Bloeß, Y. Durand, M. Matsushita, H. van der Meer, G. J. Brakenhoff and J. Schmidt, "Optical far-field microscopy of single molecules with 3.4 nm lateral resolution," *J. Microsc.*, **2002**, *205* (1); 76–85.

[20] L. Fleury, A. Gruber, A. Dräbenstedt, J. Wachtrup and C. von Borczyskowski, "Low-temperature confocal microscopy on individual molecules near a surface," *J. Phys. Chem. B*, **1997**, *101*; 7933–7938.

[21] T. Schmidt, G. J. Schütz, W. Baumgartner, H. J. Gruber and H. Schindler, "Imaging of single molecule diffusion," *Proc. Natl. Acad. Sci. USA*, **1996**, *93*; 2926–2929.

[22] A. Yildiz, J. N. Forkey, S. A. McKinney, T. Ha, Y. E. Goldman and P. R. Selvin, "Myosin V Walks Hand-Over-Hand: Single Fluorophore Imaging with 1.5-nm Localization," *Science*, **2003**, *300*; 2061–2065.

[23] K. K. Rebane, "Zero-phonon line as the foundation stone of high-resolution matrix spectroscopy, persistent spectral hole burning, single impurity molecule spectroscopy," *Chemical Physics*, **1994**, *189*; 139–148.

[24] K. K. Rebane and I. Rebane, "Peak value of the cross-section of the zero-phonon line's absorption," *J. Lumin.*, **1993**, *56*; 39–45.

[25] L. Kador, D. E. Horne and W. E. Moerner, "Optical Detection and Probing of Single Dopant Molecules of Pentacene in a *p*-Terphenyl Host Crystal by Means of Absorption Spectroscopy," *J. Phys. Chem.*, **1990**, *94*; 1237–1248.

[26] L. Kador, T. Latychevskaia, A. Renn and U. P. Wild, "Absorption spectroscopy on single molecules in solids," *J. Chem. Phys.*, **1999**, *111* (19); 8755–8758.

[27] B. Alén, F. Bickel, K. Karrai, R. J. Warburton and P. M. Petroff, "Stark-shift modulation absorption spectroscopy of single quantum dots," *Appl. Phys. Lett.*, **2003**, *83* (11); 2235–2237.

[28] T. Plakhotnik and V. Palm, "Interferometric Signatures of Single Molecules," *Phys. Rev. Lett.*, **2001**, *87* (18); 183602.

[29] W. E. Moerner and T. P. Carter, "Statistical Fine Structure of Inhomogeneously Broadened Absorption Lines," *Phys. Rev. Lett.*, **1987**, *59* (23); 2705–2708.

[30] E. A. Donley, *Single-molecule spectroscopy at subkelvin temperatures*, Ph.D. thesis, ETH Zürich, **2000**.

[31] S. Kummer, T. Basché and C. Bräuchle, "Terrylene in *p*-terphenyl: a novel single crystalline system for single molecule spectroscopy at low temperatures," *Chem. Phys. Lett.*, **1994**, *229*; 309–316.

[32] J. Y. P. Butter, B. R. Crenshaw, C. Weder and B. Hecht, "Single-Molecule Spectroscopy of Uniaxially Oriented Terrylene in Polyethylene," *ChemPhysChem*, **2006**, *7*; 261–265.

[33] J. D. Jackson, *Classical Electrodynamics*, John Wiley & Sons, Inc., 3rd edition, **1999**.

[34] L. Mandel and E. Wolf, *Optical Coherence and Quantum Optics*, Cambridge University Press, **1995**.

[35] C. F. Bohren and D. R. Huffman, *Absorption and Scattering of Light by Small Particles*, John Wiley & Sons, Inc., **1998**.

[36] H. Paul, *Photonen: Eine Einführung in die Quantenoptik*, B. G. Teubner, 2nd edition, **1995**.

[37] H. de Vries and D. A. Wiersma, "Fluorescence transient and optical free induction decay spectroscopy of pentacene in mixed crystals at 2 K. Determination of intersystem crossing and internal conversion rates." *J. Chem. Phys.*, **1979**, *70* (12); 5807–5822.

[38] T. Plakhotnik, W. E. Moerner, V. Palm and U. P. Wild, "Single molecule spectroscopy: maximum emission rate and saturation intensity," *Optics Commun.*, **1995**, *114*; 83–88.

[39] J. Bernard, L. Fleury, H. Talon and M. Orrit, "Photon bunching in the fluorescence from single molecules: A probe for intersystem crossing," *J. Chem. Phys.*, **1993**, *98* (2); 850–859.

[40] H. de Vries and D. A. Wiersma, "Photophysical and photochemical molecular hole burning theory," *J. Chem. Phys.*, **1980**, *72* (3); 1851–1863.

[41] W. P. Ambrose, T. Basché and W. E. Moerner, "Detection and spectroscopy of single pentacene molecules in a *p*-terphenyl crystal by means of fluorescence excitation," *J. Chem. Phys.*, **1991**, *95* (10); 7150–7163.

[42] R. W. Boyd, *Nonlinear optics*, Academic press, 2nd edition, **2002**.

[43] M. Born and E. Wolf, *Principles of Optics*, Cambridge university press, 7th edition, **2002**.

[44] E. Abbe, "Beiträge zur Theorie des Mikroskops und der mikroskopischen Wahrnehmung," *Archiv f. Mikroskop. Anal.*, **1873**, *9*; 413.

[45] J. B. Pawley, ed., *Handbook of biological confocal microscopy*, Plenum press, New York, 2nd edition, **1995**.

[46] S. Weiss, "Fluorescence spectroscopy of Single Biomolecules," *Science*, **1999**, *283*; 1676–1683.

[47] R. H. Webb, "Confocal optical microscopy," *Rep. Prog. Phys.*, **1996**, *59*; 427–471.

[48] R. Stöckle, C. Fokas, V. Deckert, R. Zenobi, B. Sick, B. Hecht and U. P. Wild, "High-quality near-field optical probes by tube etching," *Appl. Phys. Lett.*, **1999**, *75* (2); 160–162.

[49] T. Saiki, S. Mononobe, M. Ohtsu, N. Saito and J. Kusano, "Tailoring a high-transmission fiber probe for photon scanning tunneling microscope," *Appl. Phys. Lett.*, **1996**, *68* (19); 2612–2614.

[50] G. A. Valaskovic, M. Holton and G. M. Morrison, "Parameter control, characterization and optimization in the fabrication of optical fiber near-field probes," *Appl. Opt.*, **1995**, *34* (7); 1215–1228.

[51] A. Harootunian, E. Betzig, M. Isaacson and A. Lewis, "Super-resolution fluorescence near-field scanning optical microscopy," *Appl. Phys. Lett.*, **1986**, *49* (11); 674–676.

[52] E. Betzig, M. Isaacson and A. Lewis, "Collection mode near-field scanning optical microscopy," *Appl. Phys. Lett.*, **1987**, *51* (25); 2088–2090.

[53] E. Betzig, J. K. Trautman, T. D. Harris, J. S. Weiner and R. L. Kostelak, "Breaking the diffraction Barrier: Optical Microscopy of a Nanometric Scale," *Science*, **1991**, *251* (5000); 1468–1470.

[54] M. Muranishi, K. Sato, S. Hosaka, A. Kikukawa, T. Shintani and K. Ito, "Control of Aperture Size of Optical Probes for Scanning Near-Field Optical Microscopy Using Focussed Ion Beam Techniques," *Jpn. J. Appl. Phys., Part 2*, **1997**, *36* (7B); L942–L944.

[55] J. A. Veerman, A. M. Otter, L. Kuipers and N. F. van Hulst, "High definition aperture probes for near-field optical microscopy fabricated by focussed ion beam milling," *Appl. Phys. Lett.*, **1998**, *72* (24); 3115–3117.

[56] L. Novotny, D. W. Pohl and B. Hecht, "Light confinement in scanning near-field optical microscopy," *Ultramicroscopy*, **1995**, *61*; 1–9.

[57] H. A. Bethe, "Theory of Diffraction by Small Holes," *Phys. Rev.*, **1944**, *66* (7–8); 163–182.

[58] C. J. Bouwkamp, "On Bethe's Theory of Diffraction by Small Holes," *Philips Res. Rep.*, **1950**, *5* (5); 321–332.

[59] L. Novotny, D. W. Pohl and P. Regli, "Light propagation through nanometer-sized structures: the two-dimensional-aperture scanning near-field optical microscope," *J. Opt. Soc. Am. A*, **1994**, *11* (6); 1768–1779.

[60] J. A. Matteo, D. P. Fromm, Y. Yuen, P. J. Schuck, W. E. Moerner and L. Hesselink, "Spectral analysis of strongly enhanced visible light transmission through single C-shaped nanoapertures," *Appl. Phys. Lett.*, **2004**, *85* (4); 648–650.

[61] J.-M. Segura, A. Renn and B. Hecht, "A sample-scanning confocal optical microscope for cryogenic operation," *Rev. Sci. Instrum.*, **2000**, *71* (4); 1706–1711.

[62] J.-M. Segura, *Scanning confocal optical microscopy of single molecules at low temperature*, Ph.D. thesis, ETH Zürich, **2001**.

[63] T. M. Tritt, D. J. Gillespie, G. N. Kamm and A. C. Ehrlich, "Response of piezoelectric bimorphs as a function of temperature," *Rev. Sci. Instrum.*, **1987**, *58* (5); 780–783.

[64] C. Renner, P. Niedermann, A. D. Kent and O. Fisher, "A vertical piezoelectric inertial slider," *Rev. Sci. Instrum.*, **1990**, *61* (3); 965–967.

[65] D. W. Pohl, "Dynamic piezoelectric translation devices," *Rev. Sci. Instrum.*, **1987**, *58* (1); 54–57.

[66] J. W. Lyding, S. Skala, J. S. Hubacek, R. Brockenbrough and G. Gammie, "Variable-temperature scanning tunneling microscope," *Rev. Sci. Instrum.*, **1988**, *59* (9); 1897–1902.

[67] G. Mariotto, M. D'Angelo and I. V. Shvets, "Dynamic behavior of a piezowalker, inertial and frictional configurations," *Rev. Sci. Instrum.*, **1999**, *70* (9); 3651–3655.

[68] C. L. Jahncke and H. D. Hallen, "A versatile stable scanning proximal probe microscope," *Rev. Sci. Instrum.*, **1997**, *68* (4); 1759–1763.

[69] D. V. Pelekhov, J. B. Becker and G. N. Jr., "Ultralow-temperature atomic force microscopy for the investigation of mesoscopic systems," *Appl. Phys. Lett.*, **1998**, *72* (8); 993–995.

[70] P. Muralt, D. W. Pohl and W. Denk, "Wide-range, low-operating-voltage, bimorph STM: Application as potentiometer," *IBM J. Res. Dev.*, **1986**, *30* (5); 443–450.

[71] W. Göhde, J. Tittel, T. Basché, C. Bräuchle, U. C. Fischer and H. Fuchs, "A low-temperature scanning confocal and near-field optical microscope," *Rev. Sci. Instrum.*, **1997**, *68* (6); 2466–2474.

[72] A. Kramer, J.-M. Segura, A. Hunkeler, A. Renn and B. Hecht, "A cryogenic scanning near-field optical microscope with shear-force gapwidth control," *Rev. Sci. Instrum.*, **2002**, *73* (8); 2937–2941.

[73] K. Karrai and R. D. Grober, "Piezoelectric tip-sample distance control for near field optical microscopes," *Appl. Phys. Lett.*, **1995**, *66* (14); 1842–1844.

[74] K. Karraï and R. D. Grober, "Piezo-electric tuning fork tip-sample distance control for near field optical microscopes," *Ultramicroscopy*, **1995**, *61*; 197–205.

[75] A. Crottini, J. L. Staehli, B. Deveaud, X. L. Wang and M. Ogura, "Ultra stable tuning fork sensor for low-temperature near-field spectroscopy," *Ultramicroscopy*, **2002**, *90*; 97–101.

[76] A. G. T. Ruiter, K. O. van der Werf, J. A. Veerman, M. F. Garcia-Parajo, W. H. J. Rensen and N. F. van Hulst, "Tuning fork shear-force feedback," *Ultramicroscopy*, **1998**, *71*; 149–157.

[77] J. Rychen, T. Ihn, P. Studerus, A. Herrmann, K. Ensslin, H. J. Hug, P. J. A. van Schendel and H. J. Güntherodt, "Operation characteristics of piezoelectric quartz tuning forks in high magnetic fields at liquid helium temperatures," *Rev. Sci. Instrum.*, **2000**, *71* (4); 1695–1697.

[78] J. Salvi, P. Chevassus, A. Mouflard, S. Davy, M. Spajer, D. Courjon, K. Hjort and L. Rosengren, "Piezoelectric shear force detection: A geometry avoidung critical tip/tuning fork gluing," *Rev. Sci. Instrum.*, **1998**, *69* (4); 1744–1746.

[79] D. Mulin, C. Vannier, C. Bainier, D. Courjon and M. Spajer, "Easy-to-use unglued tip replacement near-field optical microscope with piezoelectric shear force detection," *Rev. Sci. Instrum.*, **2000**, *71* (9); 3441–3443.

[80] P. Mühlschlegel, J. Toquant, D. W. Pohl and B. Hecht, "Glue-free tuning fork shear-force microscope," *Rev. Sci. Instrum.*, **2006**, *77*; 016105.

[81] S. Kummer, F. Kulzer, R. Kettner, T. Basché, C. Tietz, C. Glowatz and C. Kryschi, "Absorption, excitation and emission spectroscopy of terrylene in *p*-terphenyl: Bulk measurements and single molecule studies," *J. Chem. Phys.*, **1997**, *107* (19); 7673–7684.

[82] P. Bordat and R. Brown, "Molecular mechanisms of photo-induced spectral diffusion of single terrylene molecules in *p*-terphenyl," *J. Chem. Phys.*, **2002**, *116* (1); 229–236.

[83] P. Tchénio, A. B. Myers and W. E. Moerner, "Vibrational analysis of the dispersed fluorescence from single molecules of terrylene in polyethylene," *Chem. Phys. Lett.*, **1993**, *213* (3,4); 325–332.

[84] P. Tchénio, A. B. Myers and W. E. Moerner, "Optical studies of single terrylene molecules in polyethylene," *J. Lumin.*, **1993**, *56*; 1–14.

[85] L. Fleury, A. Zumbusch, M. Orrit, R. Brown and J. Bernard, "Optical studies of single terrylene molecules in polyethylene," *J. Lumin.*, **1993**, *56*; 15–28.

[86] E. A. Donley and T. Plakhotnik, "Spectral diffusion in polyethylene: Single-molecule studies performed between 30 mK and 1.8 K," *J. Chem. Phys.*, **2000**, *113* (20); 9294–9299.

[87] J. Y. P. Butter and B. Hecht, "Aperture scanning near-field optical microscopy and spectroscopy of single terrylene molecules at 1.8 K," *Nanotechnology*, **2006**, *17* (6); 1547–1550.

[88] P. R. Bevington and D. K. Robinson, *Data reduction and error analysis for the physical sciences*, WCB/McGraw-Hill, 2nd edition, **1992**.

[89] P. Brémaud, *An introdcution to probablistic modeling*, Springer-Verlag, **1994**.

[90] D. J. Wineland, W. M. Itano and J. C. Bergquist, "Absorption spectroscopy at the limit: detection of a single atom," *Opt. Lett.*, **1987**, *12* (6); 389–391.

[91] T. Plakhotnik, "Absorption and coherent emission of single molecules," *J. Lumin.*, **2002**, *98*; 57–62.

[92] T. Plakhotnik, "Fluctuations and Single Molecules," *Israel Journal of Chemistry*, **2004**, *44*; 373–384.

[93] T. V. Plakhotnik, "Detection of Single Molecules with a Scanning Near-Field Optical Microscope: Absorption and Luminescence," *Opt. Spectrosc. (USSR)*, **1995**, *79* (5); 688–695.

[94] T. Matsumoto, M. Ohtsu, K. Matsuda, T. Saiki, H. Saito and K. Nishi, "Low-temperature near-field nonlinear absorption spectroscopy of InGaAs single quantum dots," *Appl. Phys. Lett.*, **1999**, *75* (21); 3246–3248.

[95] J. R. Guest, T. H. Stievater, X. Li, J. Cheng, D. G. Steel, D. Gammon, D. S. Katzer, D. Park, C. Ell, A. Thränhardt, G. Khitrva and H. M. Gibbs, "Measurement of optical absorption by a single quantum dot exciton," *Phys. Rev. B*, **2002**, *65*; 241310(R).

[96] A. Kiraz, M. Ehrl, C. Bräuchle and A. Zumbusch, "Low temperature single molecule spectroscopy using vibronic excitation and dispersed fluorescence detection," *J. Chem. Phys.*, **2003**, *118* (24); 10821–10824.

[97] A. Kiraz, M. Ehrl, C. Hellriegel, C. Bräuchle and A. Zumbusch, "Vibronic Excitation of Single Molecules: A New Technique for Studying Low-Temperature Dynamics," *ChemPhysChem*, **2005**, *6*; 919–925.

[98] H. Bach, *Spectral dynamics of single molecules*, Ph.D. thesis, ETH Zürich, **1998**.

[99] J. Michl and E. W. Thulstrup, *Spectroscopy with polarized Light*, VHC Publishers, 1st edition, **1986**.

[100] M. Grell and D. D. C. Bradley, "Polarized Luminescence from Oriented Molecular Materials," *Adv. Mater.*, **1999**, *11* (11); 895–905.

[101] M. Eglin, A. Montali, A. R. A. Palmans, T. Tervoort, P. Smith and C. Weder, "Ultra-high performance photoluminescent polarizers based on melt-processed polymer blends," *J. Mater. Chem.*, **1999**, *9*; 2221–2226.

[102] W. Trabesinger, A. Renn, B. Hecht, U. P. Wild, A. Montali, P. Smith and C. Weder, "Single-Molecule Imaging Revealing the Deformation-Induced Formation of a Molecular Polymer Blend," *J. Phys. Chem. B*, **2000**, *104*; 5221–5224.

[103] M. Orrit, J. Bernard, A. Zumbusch and R. I. Personov, "Stark effect on single molecules in a polymer matrix," *Chem. Phys. Lett.*, **1992**, *196* (6); 595–600.

[104] A. C. Wirtz, M. Dokter, C. Hofmann and E. J. J. Groenen, "Spincoated polyethylene films for single-molecule optics," *Chem. Phys. Lett.*, **2006**, *417*; 383–388.

[105] J. Sepioł, J. Jasny, J. Keller and U. P. Wild, "Single molecules observed by immersion mirror objective. The orientation of terrylene molecules via the direction of its transition dipole moment," *Chem. Phys. Lett.*, **1997**, *273*; 444–448.

[106] E. H. Synge, "A suggested model for extending microscopic resolution into the ultra-microscopic region," *Phil. Mag.*, **1928**, *6*; 356–362.

[107] J. A. Veerman, M. F. Garcia-Parajo, L. Kuipers and N. F. van Hulst, "Single molecule mapping of the optical field distribution of probes for near-field microscopy," *J. Microsc.*, **1999**, *194* (2/3); 477–482.

[108] R. C. Dunn, "Near-Field Scanning Optical Microscopy," *Chem. Rev.*, **1999**, *99*; 2891–2927.

[109] B. Hecht, B. Sick, U. P. Wild, V. Deckert, R. Zenobi, O. J. F. Martin and D. W. Pohl, "Scanning near-field optical microscopy with aperture probes: Fundamentals and applications," *J. Chem. Phys.*, **2000**, *112* (18); 7761–7774.

[110] T. D. Harris, D. Gershoni, L. Pfeiffer, M. Nirmal, J. K. Trautman and J. J. Macklin, "High spatial resolution spectroscopy of single semiconductor nanostructures," *Semicond. Sci. Technol.*, **1996**, *11*; 1569–1574.

[111] F. Intonti, V. Emiliani, C. Lienau, T. Elsaesser, R. Nötzel and K. H. Ploog, "Low temperature near-field luminescence studies of localized and delocalized excitons in quantum wires," *J. Microsc.*, **2001**, *202* (1); 193–201.

[112] A. Feltrin, R. I. Kaitouni, A. Crottini, M.-A. Dupertuis, J. Staehli, B. Deveaud, V. Savona, X. Wang and M. Ogura, "Exciton relaxation and level repulsion in GaAs/$Al_xGa_{1-x}As$ quantum wires," *Phys. Rev. B*, **2004**, *69*; 205321.

[113] M. Brun, S. Huant, J. C. Woehl, J.-F. Motte, L. Marsal and H. Mariette, "Low-temperature near-field spectroscopy of CdTe quantum dots," *J. Microsc.*, **2001**, *202* (1); 202–208.

[114] K. Matsuda, T. Saiki, S. Nomura, M. Mihara, Y. Aoyagi, S. Nair and T. Takagahara, "Near-Field Optical Mapping of Exciton Wave Functions in a GaAs Quantum Dot," *Phys. Rev. Lett.*, **2003**, *91* (17); 177401.

[115] R. D. Grober, T. D. Harris, J. K. Trautman and E. Betzig, "Design and implementation of a low temperature near-field scanning optical microscope," *Rev. Sci. Instrum.*, **1994**, *65* (3); 626–631.

[116] Y. Durand, J. C. Woehl, B. Viellerobe, W. Göhde and M. Orrit, "New design of a cryostat-mounted scanning near-field optical microscope for single molecule spectroscopy," *Rev. Sci. Instrum.*, **1999**, *70* (2); 1318–1325.

[117] R. D. Grober, T. D. Harris, J. K. Trautman, E. Betzig, W. Wegschneider, L. Pfeffer and K. West, "Optical spectroscopy of GaAs/AlGaAs quantum wire structure using near-field scanning optical microscopy," *Appl. Phys. Lett.*, **1994**, *64* (11); 1421–1423.

[118] W. P. Ambrose, P. M. Goodwin, J. C. Martin and R. A. Keller, "Alterations of Single Molecule Fluorescence Lifetimes in Near-field Optical Microscopy," *Science*, **1994**, *265* (5170); 364–367.

[119] X. S. Xie and R. C. Dunn, "Probing Single Molecule Dynamics," *Science*, **1994**, *265* (5170); 361–364.

[120] R. X. Bian, R. C. Dunn, X. S. Xie and P. T. Leung, "Single Molecule Emission Characteristics in Near-Field Microscopy," *Phys. Rev. Lett.*, **1995**, *75* (26); 4772–4775.

Curriculum Vitae

Name:	Jacqueline Yvonne Paula Butter
Date of birth:	September 16, 1980
Place of birth:	Heemstede, The Netherlands
Nationality:	Dutch

Education

09/1991 – 06/1997	Gymnasium in Lisse, The Netherlands
09/1997 – 04/2002	Studies at Leiden University, The Netherlands
08/1998	"Propaedeuse" in mathematics and astronomy.
04/2000 – 06/2000	Research assistant in the group of Prof. J. P. Woerdman on "Polarisation instabilities in Vertical Cavity Surface Emitting Lasers (VCSELs) as a function of temperature".
09/2000 – 06/2001	Research assistant in the group of Dr. E. J. J. Groenen and Prof. J. Schmidt on "A single-molecule study of the Shpol'skii system 2.3,8.9-dibenzanthanthrene in n-decane".

08/2001 – 12/2001	Master thesis in the group of Prof. T. Schmidt on "Mobility in membranes studied by Fluorescence Recovery after Photo-bleaching".
01/2002 – 03/2002	Erasmus scholarship. Research assistant at the "Centre de Physique Moléculaire Optique et Herzienne" in Bordeaux (Université de Bordeaux 1), France, in the group of Prof. B. Lounis in collaboration with the group of Prof. D. Choquet at the Université de Bordeaux 2. Topic: "Comparison of the photophysical properties of single yellow- and citrine-fluorescent proteins in the membranes of living cells".
04/2002	M.Sc. degree in physics. Grade: Cum Laude (highest grade).
05/2002 – 04/2006	Ph.D. student in the group of Prof. B. Hecht at the Institute for Physics of the University of Basel, Switzerland. Topic: "Single-molecule nano-optics at low temperature".

Teaching experience

04/2003 – 09/2005	Teaching assistant for introductory physics courses for undergraduate students of pharmacy, biology and nanoscience.

Languages

Dutch (native); Fluent in English, French and German; Very good knowledge of Italian.

Publications

From this thesis:

- J. Y. P. Butter, B. R. Crenshaw, C. Weder and B. Hecht,
  "Single-molecule spectroscopy of uniaxially oriented terrylene in polyethylene",
  Chem.Phys.Chem., **2006**, *7*; 261–265.

- J. Y. P. Butter and B. Hecht,
  "Aperture scanning near-field optical microscopy and spectroscopy of single terrylene molecules at 1.8 K",
  Nanotechnology, **2006**, *17*; 1547–1550.

- J. Y. P. Butter, B. R. Crenshaw, C. Weder and B. Hecht,
  "Absorption and fluorescence of single molecules",
  (submitted)

- J. Y. P. Butter and B. Hecht,
  "Saturation effects in single-molecule imaging",
  (in preparation)

Other:

- M. Matsushita, A. Bloess, Y. Durand, J. Y. P. Butter, J. Schmidt and E. J. J. Groenen,
  "Single molecules as nanoprobes. A study of the Shpol'skii effect"
  J. Chem. Phys., **2002**, *117*; 3383–3390.

Folgenden Dozentinnen und Dozenten der Universiteit Leiden, der Université de Bordeaux 1, der Université de Bordeaux 2 und der Universität Basel verdanke ich meine Ausbildung:
J. Aarts, T. J. Aartsma, P. van Baal, H. van Beelen, C. W. J. Beenakker, H. W. J. Blöte, P. J. M. Bongaarts, H. P. Brom, D. Choquet, P. J. H. Denteneer, E. R. Eliel, M. P. van Exter, J. W. M. Frenken, G. Frossati, P. Gast, A. M. van Genderen, J. A. van de Griend, E. J. J. Groenen, H.-J. Güntherodt, H. J. Habing, B. Hecht, L. J. F. Hermans, J. Hulshof, F. P. Israël, L. J. de Jongh, R. J. Kooman, J. Korving, W. A. Kosters, B. Lounis, W. J. A. Maaskant, J. L. Mijnheer, T. H. M. Mulder, W. L. G. A. M. van Neerven, G. J. Nieuwenhuys, G. Nienhuis, E. M. Opdam, D. W. Pohl, J. M. van Ruitenbeek, J. Schmidt, Th. Schmidt, R. Tijdeman, S. R. Völker, J. P. Woerdman.